AD-A035 036 LOCKHEED MISSILES AND SPACE CO INC HUNTSVILLE ALA HU--ETC F/G 20/5
PLASMA CHEMISTRY PROCESSES IN PULSED ELECTRIC DISCHARGE LASERS.(U)
AUG 76 J THOENES, S C KURZIUS DAAH03-75-A-0040

UNCLASSIFIED LMSC-HREC-TR-D497000 RH-CR-76-12 NL

| OF |
AD
A035036

END

DATE
FILMED
3-77

Technical Report RH-CR-76-12

LOCKHEED

PLASMA CHEMISTRY PROCESSES IN PULSED ELECTRIC DISCHARGE LASERS

Jürgen Thoenes
Shelby C. Kurzius

Lockheed Missiles & Space Company, Inc.
Huntsville Research & Engineering Center
4800 Bradford Drive
Huntsville, AL 35807

August 1976

Prepared for

High Energy Laser Systems Project Office
US Army Missile Command, Redstone Arsenal, AL 35809

Army High Energy Laser Directorate
US Army Missile Command, Redstone Arsenal, AL 35809

DISCLAIMER

The findings in this report are not to be construed as an official Department of the Army position unless so designated by other authorized documents.

DISPOSITION INSTRUCTIONS

Destroy this report when it is no longer needed. Do not return it to the originator.

TRADE NAMES

Use of trade names or manufacturers in this report does not constitute an official endorsement or approval of the use of such commercial hardware or software.

SECURITY CLASSIFICATION OF THIS PAGE (When Data Entered)

REPORT DOCUMENTATION PAGE

READ INSTRUCTIONS BEFORE COMPLETING FORM

1. REPORT NUMBER: RH-CR-76-12	2. GOVT ACCESSION NO.
3. RECIPIENT'S CATALOG NUMBER	
4. TITLE (and Subtitle): PLASMA CHEMISTRY PROCESSES IN PULSED ELECTRIC DISCHARGE LASERS.	5. TYPE OF REPORT & PERIOD COVERED: Final Report. 11 Dec 75 – 30 Aug 76.
6. PERFORMING ORG. REPORT NUMBER: LMSC-HREC-TR-D497000	
7. AUTHOR(s): Jürgen Thoenes and Shelby C. Kurzius	8. CONTRACT OR GRANT NUMBER(s): DAAH03-75-A-0040 Delivery Order CC-10
9. PERFORMING ORGANIZATION NAME AND ADDRESS: Lockheed Missiles & Space Company, Inc. Huntsville Research & Engineering Center Huntsville, Alabama 35807	10. PROGRAM ELEMENT, PROJECT, TASK AREA & WORK UNIT NUMBERS
11. CONTROLLING OFFICE NAME AND ADDRESS: 64p.	12. REPORT DATE: 30 August 1976
	13. NUMBER OF PAGES: 64
14. MONITORING AGENCY NAME & ADDRESS (if different from Controlling Office): Laser Science Division Army High Energy Laser Directorate Redstone Arsenal, AL 35812	15. SECURITY CLASS. (of this report): Unclassified
	15a. DECLASSIFICATION/DOWNGRADING SCHEDULE

16. DISTRIBUTION STATEMENT (of this Report)

Contractual Distribution List Attached

17. DISTRIBUTION STATEMENT (of the abstract entered in Block 20, if different from Report)

18. SUPPLEMENTARY NOTES

19. KEY WORDS (Continue on reverse side if necessary and identify by block number)

Repetitively Pulsed Laser
Electric Discharge
Plasma Chemistry
Electrophilic Species

20. ABSTRACT (Continue on reverse side if necessary and identify by block number)

A theoretical model is developed to analyze plasma chemistry effects on the performance of pulsed, electron-beam sustained, electric discharge lasers. Predicted single pulse performance for a CO_2^* laser oscillator at 5 atm is found to be in excellent agreement with experiment. Analysis of several potential laser gas mixtures containing hydrogen in place of helium indicated that closed cycle operation and repetitive pulsing leads to a strong degradation of laser performance due to formation of electrophilic species. Important contaminants are identified, and their selective removal is shown to prevent degradation of laser performance.

DD FORM 1 JAN 73 1473 EDITION OF 1 NOV 65 IS OBSOLETE

210 105

SECURITY CLASSIFICATION OF THIS PAGE (When Data Entered)

FOREWORD

This report presents results of work performed by the Lockheed-Huntsville Research & Engineering Center under Contract DAAH03-75-A-0040, Delivery Order CC-10, for the U.S. Army Missile Command, Redstone Arsenal, Alabama. From the administrative point of view, this document represents a final report. However, the work itself has raised a sufficient number of as yet unanswered questions such that, from the technical point of view, this should only be considered as an interim report.

This work was monitored by Mr. Charles M. Cason of the Laser Science Division, Army High Energy Laser Directorate. The period of performance covered by this report was from 11 December 1975 through 30 August 1976.

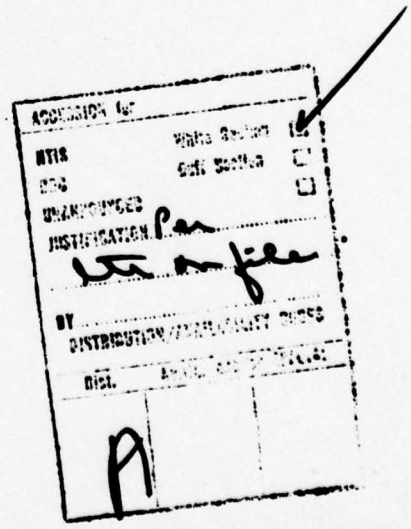

CONTENTS

Section 1
INTRODUCTION AND SUMMARY

Closed cycle operation of CO_2 electric discharge lasers has been shown to be substantially influenced by the buildup of molecular species with high electron attachment cross sections, negative ions which increase the plasma heating, and species which efficiently deactivate the upper laser level. The plasma chemistry important in the formation of these impurities has been studied in greatest detail for $He/N_2/CO_2$ mixtures loaded by a dc discharge. Current Army emphasis is on elimination of helium containing mixtures (for logistical reasons) and the development of repetitively pulsed laser technology. Thus, particularly for closed cycle operation, there exists interest in determining dominant processes detrimental to sustained repetitive high energy density pulsed loading of generic $H_2/N_2/CO_2$ laser mixtures which might also contain CO, H_2O or other species characteristic of hydrocarbon fuel combustion products.

The purpose of the effort described here was to identify chemical reactions leading to impurity production in several laser gas mixtures, to determine the relative importance of the impurity reaction products in degrading assessed laser performance, and to furnish predictions of all important molecular species production and decay rates during and following the electrical pulse. In doing this, maximum use was to be made of existing kinetic data and of the existing continuous wave electric laser code previously developed by the authors (Ref. 1).

Furthermore, the steady state buildup of impurity concentrations under repetitively pulsed operation was to be examined, and key experimental efforts to verify predicted results were to be recommended.

The essential features of the modeling approach used in this effort are described in Section 2. The discussion includes the basic equations as well

as the details of the plasma kinetics model employed. Results obtained for several laser gas mixtures are described in Section 3. Discussion of the standard $CO_2/N_2/He$ laser gas mixture includes a comparison of performance characteristics as predicted by the model developed under this contract with experimental data. The good agreement achieved lends credibility to the theoretical model and its application to the analysis of other laser gas mixtures.

Section 4 presents the conclusions derived from the work accomplished. Also presented are recommendations for key experimental efforts that should be undertaken to verify predicted results, as well as for future theoretical efforts that should be performed to develop a more user-oriented, efficient computer model specifically suited to investigate pulsed electric lasers.

Briefly summarizing, a theoretical model is presented which can be used to analyze plasma chemistry effects on the performance of pulsed, electron beam sustained electric discharge lasers. The one-dimensional model contains descriptions of the configuration components of primary importance which are the electron beam, the discharge, the plasma and its composition, laser radiation, and their mutual interaction. All important processes are modeled in terms of experimentally controllable parameters which include the post-foil electron beam current density, the primary electron energy, the applied electric field potential, discharge electrode spacing, initial laser gas composition, temperature and pressure, both electron beam and electric discharge pulse widths and relative sequencing, as well as cavity geometric data such as mirror reflectivities, transmissivities and separation.

Calculated single pulse performance for a CO_2 laser oscillator at 5 atm is found to be in good agreement with experiment. Analysis of several potential laser gas mixtures containing hydrogen in place of helium, under conditions representative for the small scale closed cycle circulator planned by the Army, indicated that closed cycle operation and repetitive pulsing leads to a strong degradation of laser performance due to formation of electrophilic species. Important contaminants are identified, and their selective removal is shown to prevent degradation of laser performance.

Section 2
MODELING APPROACH

2.1 THEORETICAL MODEL

This section presents a brief description of the essential features which a theoretical model must possess to adequately describe plasma chemistry processes in pulsed electric discharge lasers. This model incorporates descriptions of the electron beam, the discharge, the plasma composition and laser radiation, and their mutual interaction. The effect of both single and repetitive pulsing can be modeled. To simulate selective removal of detrimental species (scrubbing) the plasma composition can be modified between successive pulses when recirculation and repetitive pulsing are to be considered. Modeling as many of the basic features of a device as possible serves to minimize simplifying assumptions which always have to be made. An important simplification made in this work is the assumption of spatially uniform conditions in the cavity resulting in a one-dimensional model. On the other hand, the full coupling of the energy equation into the system of species rate equations eliminates the often made assumption (see Section 4) that variations in the gas temperature, which is of prime importance to laser operation, can be ignored.

Considering uniformly excited laser cavity volumes of the order of a few liters, and electric discharge pulses of approximately microsecond duration it can easily be shown that a constant density, time-dependent treatment of the plasma chemistry should adequately describe the important processes occurring in a pulsed discharge. For repetitively pulsed discharges and closed loop operation of the laser, the flow velocity around the cycle is assumed to be sufficiently small that pressure changes due to varying flow velocity can be neglected. Plasma composition changes around the recirculation loop can then be treated in the same time-dependent manner as in the cavity, provided that post-discharge expansion of the plasma as well as cooling by heat exchangers is appropriately accounted for.

The laser gas mixture generally consists of neutral atoms and molecules, charged atoms and molecules, vibrationally excited molecules, and electrons. Therefore a multitude of species must be tracked during the calculations. It is assumed that different quantum states of various particles can be treated as separate species. For simplicity, it is also assumed that a single vibrational-rotational radiative transition sufficiently accounts for laser output. While not generally true, this is a reasonable assumption if lasing of the CO_2 molecule is considered.

Under the above stated assumptions the basic governing equations can be written as follows:

Continuity:

$$\frac{d\rho}{dt} = 0 \tag{1}$$

Species:

$$\rho \frac{dF_i}{dt} = \dot{w}_i + (\delta_{i1} - \delta_{i2}) \frac{\alpha I}{\epsilon} \tag{2}$$

Here ρ denotes the density, F_i the mol/mass ratio of the i^{th} species, and $\dot{w}_i$ its overall net rate of production due to any reaction mechanism except for radiation. For an arbitrary reaction of the form

$$\sum_{i=1}^{N} \nu_i' A_i \rightleftharpoons \sum_{i=1}^{N} \nu_i'' A_i \tag{3}$$

the net rate of production for any participating species for which $\nu_i'' - \nu_i' \neq 0$ can be written as

$$\dot{w}_i = (\nu_i'' - \nu_i') \left\{ k_f \prod_{i=1}^{N} (\rho F_i)^{\nu_i'} - k_b \prod_{i=1}^{N} (\rho F_i)^{\nu''} \right\} \tag{4}$$

where k_f and k_b denote the forward and backward rate constant, respectively. Laser radiation, its intensity denoted by I, depletes the upper laser level and replenishes the lower laser level, as indicated by the Kronecker symbols in Eq. (2). Gain and photon energy are denoted by α and ϵ, respectively.

Energy:

$$\frac{d}{dt}(\rho e) = j_D E - \kappa \bar{\alpha} I \tag{5}$$

which simply states that any change of internal energy of the laser gas is due to discharge energy pumped into the plasma, or due to radiation leaving the gas in the cavity. Here j_D denotes the drift field current density and E the electric field strength. The quantity κ represents a correction factor and is defined as

$$\kappa \equiv \frac{1 - \exp(-\bar{\alpha}L)}{\bar{\alpha}L} \tag{6}$$

where $\bar{\alpha}$ is the cavity threshold gain. Assuming a Fabry-Perot cavity, the threshold gain can be expressed in terms of mirror reflectivities and optical path length through the gain medium as

$$\bar{\alpha} = -\frac{\ell n(r_1 r_2)}{2L} \tag{7}$$

Note that for $\bar{\alpha}L \ll 1$, which is most often the case, κ reduces to unity. Lasing commences when the medium gain exceeds the cavity gain, and ceases when the pumping reactions fail to maintain the medium gain at the cavity gain level.

The medium gain can be expressed as

$$\alpha = \rho \epsilon (S_{21} F_2 - S_{12} F_1) V \tag{8}$$

where F_2 and F_1 are the mol/mass ratios of the upper and the lower laser level, respectively. All spectroscopic data enter the equation through S_{21} and S_{12} which are functions of temperature only. V denotes the Voigt function which basically represents a generalized line shape function,

$$V(\eta) = \exp(\eta^2)\,[1 - \mathrm{erf}(\eta)] \tag{9}$$

with η being the ratio of the Lorentz line width to the Doppler line width, i.e.,

$$\eta = (\ell n 2)^{1/2} \frac{\Delta\nu_L}{\Delta\nu_D} \tag{10}$$

The set of basic equations is completed by the equation of state,

$$p = \rho \, \Re \, T \sum_{i=1}^{NS} F_i \tag{11}$$

which determines the pressure as a function of density, temperature and gas composition.

Energizing the laser gas in an electric discharge requires the presence of free electrons which are, at least initially, here assumed to be generated by electron-beam ionization. Assuming that both the effective electron-beam current density, j_{EB}, and the effective electron beam energy, E_{EB}, are specified, the number density of primary electrons in the laser gas can be expressed as

$$n_{EB} = \frac{j_{EB}}{q_e \, V_{EB}} \tag{12}$$

where q_e is the electron charge, and V_{EB} the beam electron velocity expressed as

$$V_{EB} = c \left(\frac{2 E_{EB}}{E_{REF}} \right)^{1/2} \tag{13}$$

Here c denotes the speed of light, and E_{REF} the electron rest mass energy equivalence ($m_e \, c^2 = 511$ keV). Knowing the primary electron density, the rate of ionization and production of secondary electrons due to the electron beam only can be determined according to the reaction

$$A_i + n_{EB} \xrightarrow{k_{f,i}} A_i^+ + n_e + n_{EB} \tag{14}$$

where the primary ionization rate constant, $k_{f,i}$, can be evaluated as a function of the ion mass, the beam ionizing power and the beam electron velocity (Ref. 1).

The drift field current density, and therefore the energy which can be pumped into the gas, is proportional to the number of free electrons and their drift velocity which in turn is dependent on the electrical field strength, such that, to good approximation,

$$j_D = C\, n_e\, q_e\, (E/N)^{3/4} \tag{15}$$

The volumetric rate of energy addition in the discharge can then be expressed as

$$j_D E = C\, n_e\, q_e\, N\, (E/N)^{7/4} \tag{16}$$

where the constant C, strictly speaking, is mixture-dependent, but in practice was found to be essentially independent of the gas mixture over the range of compositions considered. Equation (16) is not only used to evaluate the energy added in the discharge but also to determine the secondary electron energy which is essential in evaluating electron impact excitation rates. Postulating a basic electron impact vibrational excitation mechanism as

$$A_i(v) + e \xrightarrow{k_{f,i}} A_i(v' > v) + e \tag{17}$$

the power consumed by this mechanism can be expressed as

$$\Delta P = \sum_i n_e\, n_i\, k_{f,i}\, \Delta H_i \tag{18}$$

where the summation indicates that more than one mechanism may be involved.

Applying conservation of energy by equating the right hand sides of Eqs. (16) and (18) then leads to the important relation

$$C\, q_e\, N\, (E/N)^{7/4} = \sum_i n_i\, k_{f,i}\, \Delta H_i \qquad (19)$$

Since the impact excitation rate constants, $k_{f,i}$, are functions of the electron energy which itself is a function of E/N, Eq. (19) constitutes an implicit relation for the electron energy, and simultaneously states its functional dependence on E/N in terms of input functions.

Equations (1) through (19), in conjunction with a detailed set of reactions and rate coefficients, to be discussed in Section 2.2, provide the basic framework to evaluate plasma conditions in the discharge as a function of time, and if desired, the radiative output of the laser cavity.

In theoretically assessing the effects of recirculation on electric discharge laser performance it is most important to achieve a reasonable simulation of the density and temperature-time history around the recirculation path, because the reaction rates are essentially functions of these two parameters. The procedure followed in the present investigation was to pulse the gas in the laser cavity for the duration of microseconds at constant density. From this state of elevated pressure and temperature, the plasma is allowed to return to its initial pressure via an adiabatic expansion. The time interval appropriate for this expansion process can be estimated by considering the time which a disturbance traveling at the speed of sound would take to clear the laser cavity or discharge volume. Typically, this should occur in a time interval of the order of 100 microseconds. The theoretical cycle is completed by considering an isobaric cooling process, simulating the flow of gas through a heat exchanger, which returns the gas to the initial temperature (and pressure). Typical time intervals for this last leg of the cycle would be on the order of milliseconds.

2.2 PLASMA KINETICS

In Refs. 1 and 2 we discussed in some detail the input kinetics developed (under Contracts DAAH03-75-C-0077 and DAAH03-75-A-0040, Delivery Order

CC-11) to compute the gasdynamic, discharge and gain characteristics of a CW CO_2 electron beam-sustained discharge with air contaminant. Operation of the laser with bottled CO_2-CO-N_2-He gas mixtures of standard purity at a pressure on the order of 0.1 atm was implicitly assumed. Here we have extended the kinetics to consider repetitively pulsed operation at pressures up to 10 atm with cryogenically dried laser mixtures generated by combustion of hydrocarbon fuel with air. In this section we present the updated plasma chemistry package currently in use (Tables 1, 2 and 3) together with a very brief discussion of the changes only.

2.2.1 CO_2-CO-N_2-He Mixtures (Non-Hydrogenic)

With relatively minor modifications the plasma chemistry package of Ref. 2 has been utilized as a logical starting point for similar analysis of closed cycle pulsed operation of CO_2 electric discharge lasers utilizing 1 - 2 - 3 CO_2 - N_2 - He mixtures at atmospheric and higher pressures, with the very encouraging results discussed in Section 3. In a sense, the apparently successful extrapolation of these basic plasma kinetics to a density regime almost two orders of magnitude higher is remarkable. We had anticipated that heavy ion clustering (Ref. 3) would play a more dominant role and that as a minimum revision it would be necessary to regard the rate coefficients entered for the parent ion of a given cluster family (e.g., $CO_2^+ \cdot (CO_2)_n$) as a global, scalable descriptor for the rates of reaction of members of that particular cluster ion family. Such revisions may yet be required. It is, however, already apparent that the kinetics code provides useful predictions using inputs not radically revised from those employed in modeling plasmas at much lower pressures. To rationalize this finding, it is interesting to speculate that the heavily clustered ions observed in the recent drift tube experiments by McDaniel et al., (Ref. 3) may be unstable in the high energy density field of CO_2 laser discharges. An analogous instability of complex cluster ions in the D region of the ionosphere apparently occurs in the presence of intense solar radiation during solar flares, accounting quantitatively for observed enhanced free electron concentrations (Ref. 4).

The modifications to the non-hydrogenic kinetics inputs as listed in Ref. 2 are as follows:

Ionized Species (Table 1)

Reaction B2: In addition to the NO_2 dissociative detachment reaction B1 theoretically evaluated by Nighan and Wiegand (Ref. 5), the associative attachment process B2 forming NO_2^- has now been incorporated. Attachment coefficient B2 is the pressure-independent experimental value measured by Mahan and Walker (Ref. 6) in the presence of N_2 diluent.

Reaction C1: The associative detachment coefficient C1 for the $O^- + CO_2$ reaction has been trivially rewritten for a $T^{-0.4}$ rather than the $T^{-0.39}$ temperature dependence reported by McFarland et al (Ref. 7).

Reaction D6: Interchange reaction D6 between CO_2^+ and O atoms has been substituted for the corresponding process involving N atoms. The latter process is negligible by comparison, as is readily evident from the lower rate coefficient (viz., 5.0×10^{-12}) for this process vis a vis that for D6, each of which is from the 1973 survey by Ferguson (Ref. 8).

Reaction D28: Clustering rate coefficient D28 has been changed so that recently employed by Spjeldvik and Thorne (Ref. 9) in their D-region ionic model.

Reaction D29: The clustering reaction between C_2^- and CO_2 with O_x chaperone species has been incorporated using the rate coefficient reported by Fehsenfeld and Ferguson (Ref. 10).

Reactions E1, E2 and E3: An ion-temperature dependence has been incorporated into the very important ion-electron recombination coefficients, retaining a $u_e^{-0.5}$ electron energy dependence. In the absence of definitive data, a T^{-1} ion temperature dependence has been assumed for the more complex ions (i.e., CO_2^+ and hydrated ions), this being the limiting dependence predicted by the theoretical analysis of Bates (see e.g., Ref. 11) for

recombination in which neutral product stabilization, rather than radiationless transition, is rate-limiting. Intuitively, it seems that the multiplicity of rovibronic states available to complex ions should favor radiationless transition by increasing the overlap between bound and unbound states. For O_2^+ and NO^+ more definitive data are available, negating the need for this assumption.

Dissociative recombination coefficient E1 for CO_2^+ is based on results at 300°K cited in a review by Biondi (Ref. 12) and a T^{-1} ion temperature dependence.

Coefficient E2 for O_2^+ is based on the experimental work of Kasner and Biondi (Ref. 13).

Coefficient E3 for the process $NO^+ + e \rightarrow N + O$ has been obtained from the results at 300 K cited by Biondi (Ref. 12) combined with high temperature results cited by Hansen (Ref. 14), influenced by the $T^{-0.5}$ ion temperature dependence for coefficient E2. For the process $NO^+ + e \rightarrow NO$, actually corresponding to hydrated ion recombination, we have employed the value $1.0 \times 10^{-6} u_e^{-0.5}$ suggested by the work of Mitra and Rowe (Ref. 4), refit to a simple T^{-1} ion temperature dependence.

Reactions E4 through E21: For the most part, the ionic mutual neutralization rate coefficients, their temperature dependence, and the distribution of neutral products remain unknown. Recent merged beam results at 300 K are however, available (Ref. 15) for coefficients E8, E10, E11, E12, E14 and E15 involving O_2^+ and NO^+ neutralization with O_2^-, NO_2 and NO_3^-, and have been incorporated into Table 1. The remaining coefficients have of necessity been roughly estimated by scaling of these few measurements by the reciprocal square root of the reduced mass of the interacting ions within the positive ion groupings O_2^+, NO^+ and CO_2^+. On the basis of the empirical observation that the mean ratio of the measured O_2^+ mutual neutralization coefficients to the corresponding NO^+ coefficients is on the order of the corresponding ratio of the ion-free electron recombination coefficients at 300 K, the completely unknown ion-ion rates involving CO_2^+ were estimated on the basis of the

corresponding ratio of the CO_2^+ to O_2^+ dissociative recombination coefficients, also scaling via the reduced mass effect.

As a final caveat, it is necessary to point out that three-body Thompson ion-ion recombination (i.e., $A^+ + B^- + M \rightarrow A + B + M$) has not yet been incorporated into Table 1 but may play a significant role in the ion-ion neutralization kinetics at the relatively high pressure of interest in practical high energy discharge lasers. Theoretical work by Flannery (Ref. 16) indicates that at pressures on the order of an atmosphere ternary recombination may be more rapid than binary mutual neutralization processes.

Excited Species (Table 2): Reactions A1 and A4. The effective rate coefficients for these important vibrational pumping reactions are improved numerical fits to the results computed by Nighan (Ref. 17) largely using electron energy distributions calculated for a 1-2-3 CO_2-N_2-He mixture. The previous numerical fit (i.e., that given in Refs. 1 and 2) for rate coefficient A1 was not well-behaved at values of u_e below ~0.45 eV, while that for A4 was needlessly complex. We stress again that the coefficients A1 through A4 are somewhat mixture-dependent. For purposes of exploring the plasma chemistry the relatively slight effects of neglecting this dependence have been ignored.

2.2.2 Combustion Gas Mixtures (Hydrogenic)

With respect to CO_2 - CO-N_2-He laser mixtures with a low level of air contaminant the primary inlet composition changes in dried laser mixtures generated by combustion of hydrocarbon lie simply in the presence of a few percent of H_2, a few hundred parts per million of both NO and unburned hydrocarbon and the absence of He (Ref. 18). As an adequate simplification we assume the unburned hydrocarbon to be CH_2O (i.e., formaldehyde), a common combustion intermediate.

As we will show in Section 3, these simple changes are predicted to be sufficient to ensure that detrimental levels of strongly electrophilic species

(primarily HNO_3 and HNO_2) are formed in the post electrical pulse dwell time. The extensions to the kinetics inputs utilized in this analysis are as follows:

Ionized Species (Table 1)

- Attachment Reactions

Reaction B10: Nighan and Wiegand (Ref. 5) have theoretically evaluated the effective water dissociative electron attachment coefficient, B10, for the products OH + H^-. To avoid the necessity of accounting for H^- we have here simply written the products as OH^- + H. Coefficient B10 is a numerical fit to Nighan and Wiegand's results.

Reactions B11, B12 and B13: Fehsenfeld, Howard and Schmeltekopf (Ref. 19) have recently reported that the attachment coefficient of thermal electrons to nitric acid at 298 K is $(5 \pm 3) \times 10^{-8}$ cm^3 sec^{-1}. We have accepted this value and estimated that the analogous processes for attachment to HNO_2 and N_2O_5 are equally rapid, especially for relatively hot (i.e., $u_e > 0.5$ eV) electrons.

- Detachment Reactions

Extension to hydrogenic systems is straightforward via Reactions C9 through C12. The extensive work of Ferguson, Fehsenfeld and co-workers at the Boulder Aeronomy Laboratory is the mother lode for the rate coefficients of these reactions: C9 - Ref. 7; C10 and C11 - Ref. 20; C12 - Ref. 21.

- Charge Transfer, Interchange and Clustering Reactions

Similarly, results of the Aeronomy Laboratory are largely adequate to extend these reactions to hydrogenic systems, the sources of the rate coefficients being as follows: D36, D37 and D43 - Ref. 8 (coefficient D38 has been estimated to be approximately equal to that for the generically similar CO_2^+ metathesis D37, leading also to HCO_2^+); D44, D47, D50 and D52 - Ref. 19;

Table 1

IONIZED SPECIES REACTIONS* AND RATE COEFFICIENTS**
FOR THE CO_2 ELECTRIC DISCHARGE LASER

	A. Ionization Reactions	Rate Coefficient
A1	$CO_2(000) + e_{EB} \longrightarrow CO_2^+ + e + e_{EB}$	$6.9 \times 10^{-7}\ E_{EB}^{-2.0}$
A2	$CO(0) + e_{EB} \longrightarrow CO^+ + e + e_{EB}$	$4.0 \times 10^{-7}\ E_{EB}^{-0.2}$
A3	$N_2(0) + e_{EB} \longrightarrow N_2^+ + e + e_{EB}$	$3.7 \times 10^{-7}\ E_{EB}^{-0.2}$
A4	$He + e_{EB} \longrightarrow He^+ + e + e_{EB}$	$6.5 \times 10^{-8}\ E_{EB}^{-0.2}$
A5	$NO + e \longrightarrow NO^+ + e + e$	$4.3 \times 10^{-6}\ u_e^{-4.8}\ \exp(-15/u_e)$
A6	$CO_2(000) + e \longrightarrow CO_2^+ + e + e$	$1.7 \times 10^{-5}\ u_e^{-6.3}\ \exp(-19/u_e)$
A7	$O_2 + e \longrightarrow O_2^+ + e + e$	$1.5 \times 10^{-5}\ u_e^{-6.3}\ \exp(-19/u_e)$
A8	$N_2(0) + e \longrightarrow N_2^+ e + e$	$7.2 \times 10^{-4}\ u_e^{-10}\ \exp(-25.4/u_e)$
A9	$CO(0) + e \longrightarrow CO^+ + e + e$	$1.5 \times 10^{-5}\ u_e^{-6.0}\ \exp(-20.3/u_e)$
A10	$O_2 + e_{EB} \longrightarrow O_2^+ + e + e_{EB}$	$4.2 \times 10^{-7}\ E_{EB}^{-0.2}$
	B. Attachment Reactions	
B1	$NO_2 + e \longrightarrow O^- + NO$	$3.4 \times 10^{-10}\ u_e^{-2.4}\ \exp(-3.0/u_e)$
B2	$NO_2 + e \longrightarrow NO_2^-$	4.0×10^{-11}
B3	$O_2 + e \longrightarrow O^- + O$	$2.8 \times 10^{-6}\ u_e^{-7.9}\ \exp(-13.5/u_e)$
B4	$O_3 + e \longrightarrow O^- + O_2$	4.0×10^{-11}
B5	$NO + e \longrightarrow O^- + N$	$3.4 \times 10^{-6}\ u_e^{-8.2}\ \exp(-15.2/u_e)$
B6	$CO_2(000) + e \longrightarrow O^- + CO(0)$	$8.4 \times 10^{-8}\ u_e^{-6.4}\ \exp(-11.6/u_e)$

*All forward reactions only

**Units are as follows: Rate coefficients, cm^3-particle-sec units; E_{EB}, keV; u_e, eV; T, ^oK; R, cal-mole^{-1} - $^oK^{-1}$. (u_e is the reduced average electron energy, i.e., $u_e = k\,T_e$).

B7	$O + e + M_1 \longrightarrow O^- + M_1$	1.0×10^{-31}
B8	$O_2 + e + M_2 \longrightarrow O_2^- + M_2$	1.0×10^{-31}
B9	$O_2 + e + M_3 \longrightarrow O_2^- + M_3$	$4.2 \times 10^{-27} T^{-1} \exp(-1200/RT)$
B10	$H_2O + e \longrightarrow OH^- + H$	$2.8 \times 10^{-6} u^{-7.2} \exp(-12.9/u_e)$
B11	$HNO_3 + e \longrightarrow NO_2^- + OH$	5.0×10^{-8}
B12	$HNO_2 + e \longrightarrow NO_2^- + H$	5.0×10^{-8}
B13	$N_2O_5 + e \longrightarrow NO_3^- + NO_2$	5.0×10^{-8}

C. Detachment Reactions

C1	$O^- + CO(0) \longrightarrow e + CO_2(020)$	$5.8 \times 10^{-9} T^{-0.4}$
C2	$O^- + O \longrightarrow e + O_2$	1.9×10^{-10}
C3	$O^- + NO \longrightarrow e + NO_2$	$1.8 \times 10^{-8} T^{-0.75}$
C4	$O^- + N \longrightarrow e + NO$	2.2×10^{-10}
C5	$O_2^- + O \longrightarrow e + O_3$	3.3×10^{-10}
C6	$O_2^- + N \longrightarrow e + NO_2$	4.0×10^{-10}
C7	$O_3^- + O \longrightarrow e + O_2 + O_2$	1.0×10^{-10}
C8	$O_3^- + O_3 \longrightarrow e + O_3\ O_3$	1.0×10^{-10}
C9	$O^- + H_2 \longrightarrow H_2O + e$	$2.5 \times 10^{-9} T^{-0.25}$
C10	$OH^- + H \longrightarrow H_2O + e$	1.8×10^{-9}
C11	$OH^- + O \longrightarrow HO_2 + e$	2.0×10^{-10}
C12	$O_2^- + H \longrightarrow HO_2 + e$	1.5×10^{-9}

D. Charge Transfer, Interchange and Clustering Reactions

D1	$He^+ + CO_2(000) \longrightarrow CO^+ + O + He$	1.2×10^{-9}
D2	$N_2^+ + CO_2(000) \longrightarrow CO_2^+ + N_2(0)$	1.0×10^{-9}
D3	$CO^+ + CO_2(000) \longrightarrow CO_2^+ + CO(0)$	1.2×10^{-9}
D4	$CO_2^+ + O_2 \longrightarrow O_2^+ + CO_2(000)$	$1.1 \times 10^{-14} T \exp(1800/RT)$

D5	$CO_2^+ + NO \longrightarrow NO^+ + CO_2(000)$	1.2×10^{-10}
D6	$CO_2^+ + O \longrightarrow O_2^+ + CO(0)$	2.6×10^{-10}
D7	$O_2^+ + NO \longrightarrow NO^+ + O_2$	4.5×10^{-10}
D8	$O_2^+ + N \longrightarrow NO^+ + O$	1.8×10^{-10}
D9	$O^- + O_3 \longrightarrow O_3^- + O$	5.3×10^{-10}
D10	$O^- + NO_2 \longrightarrow NO_2^- + O$	1.2×10^{-9}
D11	$O^- + O_2 + M_1 \longrightarrow O_3^- + M_1$	$3.0 \times 10^{-28}\ T^{-1}$
D12	$O^- + NO + M_1 \longrightarrow NO_2^- + M_1$	$3.0 \times 10^{-28}\ T^{-1}$
D13	$O^- + CO_2(000) + M_1 \longrightarrow CO_3^- + M_1$	$5.0 \times 10^{-25}\ T^{-1}$
D14	$O^- + O_2 + M_4 \longrightarrow O_3^- + M_4$	2.0×10^{-30}
D15	$O_2^- + O_3 \longrightarrow O_3^- + O_2$	3.0×10^{-10}
D16	$O_2^- + NO_2 \longrightarrow NO_2^- + O_2$	1.2×10^{-9}
D17	$O_2^- + O + M_1 \longrightarrow O_3^- + M_1$	$3.0 \times 10^{-28}\ T^{-1}$
D18	$O_2^- + NO + M_1 \longrightarrow NO_3^- + M_1$	$3.0 \times 10^{-28}\ T^{-1}$
D19	$O_3^- + O \longrightarrow O_2^- + O_2$	1.0×10^{-10}
D20	$O_3^- + CO_2(000) \longrightarrow CO_3^- + O_2$	6.0×10^{-10}
D21	$O_3^- + NO \longrightarrow NO_3^- + O$	1.0×10^{-11}
D22	$O_3^- + NO_2 \longrightarrow NO_3^- + O_2$	2.8×10^{-10}
D23	$CO_3^- + O \longrightarrow O_2^- + CO_2(020)$	8.0×10^{-11}
D24	$CO_3^- + NO \longrightarrow NO_2^- + CO_2(020)$	1.8×10^{-11}
D25	$CO_3^- + NO_2 \longrightarrow NO_3^- + CO_2(000)$	2.0×10^{-10}
D26	$NO_2^- + NO_3 \longrightarrow NO_3^- + NO_2$	3.0×10^{-10}
D27	$NO_2^- + O_3 \longrightarrow NO_3^- + O_2$	1.8×10^{-11}
D28	$O_2^- + O_2 + M_1 \longrightarrow O_4^- + M_1$	$2.0 \times 10^{-27}\ T^{-1.5}$

D29	$O_2^- + CO_2(000) + M_3 \longrightarrow CO_4^- + M_3$	5.2×10^{-29}
D30	$O_4^- + O \longrightarrow O_3^- + O_2$	4.0×10^{-10}
D31	$O_4^- + CO_2(000) \longrightarrow CO_4^- + O_2$	4.8×10^{-10}
D32	$O_4^- + NO \longrightarrow NO_3^- + O_2$	2.5×10^{-10}
D33	$CO_4^- + O \longrightarrow CO_3^- + O_2$	1.5×10^{-10}
D34	$CO_4^- + NO \longrightarrow NO_3^- + CO_2(000)$	4.8×10^{-11}
D35	$CO_4^- + O_3 \longrightarrow O_3^- + CO_2(000) + O_2$	1.3×10^{-10}
D36	$CO_2^+ + H \longrightarrow HCO^+ + O$	6.0×10^{-10}
D37	$CO_2^+ + H_2 \longrightarrow HCO_2^+ + H$	1.4×10^{-9}
D38	$CO_2^+ + H_2O \longrightarrow HCO_2^+ + OH$	1.4×10^{-9}
D39	$HCO^+ + NO \longrightarrow NO^+ + CHO$	1.2×10^{-10}
D40	$HCO^+ + H_2O \longrightarrow H_3O^+ + CO(1)$	3.0×10^{-9}
D41	$HCO_2^+ + CO(0) \longrightarrow HCO^+ + CO_2(020)$	3.0×10^{-9}
D42	$HCO_2^+ + H_2O \longrightarrow H_3O^+ + CO_2(020)$	3.0×10^{-9}
D43	$O^- + H_2O \longrightarrow OH^- + OH$	1.4×10^{-9}
D44	$O^- + HNO_3 \longrightarrow NO_3^- + OH$	3.0×10^{-9}
D45	$OH^- + NO_2 \longrightarrow NO_2^- + OH$	1.9×10^{-9}
D46	$O_2^- + OH \longrightarrow OH^- + O_2$	6.0×10^{-10}
D47	$O_2^- + HNO_3 \longrightarrow NO_3^- + HO_2$	2.8×10^{-9}
D48	$O_3^- + H \longrightarrow OH^- + O_2$	8.4×10^{-10}
D49	$NO_2^- + H \longrightarrow OH^- + NO$	3.7×10^{-10}
D50	$NO_2^- + HNO_3 \longrightarrow NO_3^- + HNO_2$	1.6×10^{-9}
D51	$CO_3^- + H \longrightarrow OH^- + CO_2(000)$	1.7×10^{-10}
D52	$CO_3^- + HNO_3 \longrightarrow NO_3^- + OH + CO_2(000)$	8.0×10^{-10}
D53	$CO_4^- + H \longrightarrow CO_3^- + OH$	2.2×10^{-10}

E. Recombination Reactions

E1	$CO_2^+ + e \longrightarrow CO(1) + O$	$2.0 \times 10^{-5}\ T^{-1.0}\ u_e^{-0.5}$
E2	$O_2^+ + e \longrightarrow O + O$	$6.0 \times 10^{-7}\ T^{-0.5}\ u_e^{-0.5}$
E3*	$NO^+ + e \longrightarrow N + O$	$1.2 \times 10^{-6}\ T^{-0.5}\ u_e^{-0.5}$
E3**	$NO^+ + e \longrightarrow NO$	$3.0 \times 10^{-4}\ T^{-1.0}\ u_e^{-0.5}$
E4	$CO_2^+ + O_2^- \longrightarrow CO(1) + O_2 + O$	6.0×10^{-7}
E5	$CO_2^+ + CO_3^- \longrightarrow CO_2(020) + O + CO_2(020)$	5.0×10^{-7}
E6	$CO_2^+ + NO_2^- \longrightarrow CO(1) + O + NO_2$	6.0×10^{-7}
E7	$CO_2^+ + NO_3^- \longrightarrow CO(1) + O + NO_3$	5.0×10^{-7}
E8	$O_2^+ + O_2^- \longrightarrow O_2 + O + O$	4.0×10^{-7}
E9	$O_2^+ + CO_3^- \longrightarrow O_2 + O + CO_2(020)$	3.0×10^{-7}
E10	$O_2^+ + NO_2^- \longrightarrow O + O + NO_2$	4.0×10^{-7}
E11	$O_2^+ + NO_3^- \longrightarrow O + O + NO_3$	1.3×10^{-7}
E12	$NO^+ + O_2^- \longrightarrow N + O + O_2$	6.0×10^{-7}
E13	$NO^+ + CO_3^- \longrightarrow NO + O + CO_2(020)$	6.0×10^{-7}
E14	$NO^+ + NO_2^- \longrightarrow N + O + NO_2$	5.0×10^{-7}
E15	$NO^+ + NO_3^- \longrightarrow N + O + NO_3$	8.0×10^{-7}
E16	$CO_2^+ + O_4^- \longrightarrow CO_2(020) + O_2 + O_2$	5.0×10^{-7}
E17	$CO_2^+ + CO_4^- \longrightarrow CO_2(020) + CO_2(020) + O_2$	5.0×10^{-7}
E18	$O_2^+ + O_4^- \longrightarrow O_2 + O_2 + O_2$	3.0×10^{-7}
E19	$O_2^+ + CO_4^- \longrightarrow O_2 + CO_2(020) + O_2$	3.0×10^{-7}
E20	$NO^+ + O_4^- \longrightarrow NO + O_2 + O_2$	6.0×10^{-7}
E21	$NO^+ + CO_4^- \longrightarrow NO + CO_2(020) + O_2$	6.0×10^{-7}

*Dry

**Moist

E22	$HCO^+ + e \longrightarrow H + CO(1)$	$1.0 \times 10^{-5}\ T^{-1}\ u_e^{-0.5}$
E23	$HCO_2^+ + e \longrightarrow H + CO_2(020)$	$4.0 \times 10^{-5}\ T^{-1}\ u_e^{-0.5}$
E24	$H_3O^+ + e \longrightarrow H + H + OH$	$4.0 \times 10^{-6}\ T^{-0.5}\ u_e^{-0.5}$
E25	$HCO^+ + O_2^- \longrightarrow CO(1) + H + O_2$	3.0×10^{-7}
E26	$HCO^+ + CO_3^- \longrightarrow CO(1) + CO_2(020) + OH$	3.0×10^{-7}
E27	$HCO^+ + CO_4^- \longrightarrow CO(1) + CO_2(020) + HO_2$	3.0×10^{-7}
E28	$HCO_2^+ + O_2^- \longrightarrow CO_2(020) + H + O_2$	1.2×10^{-6}
E29	$HCO_2^+ + CO_3^- \longrightarrow CO_2(020) + CO_2(020) + OH$	1.0×10^{-6}
E30	$HCO_2^+ + CO_4^- \longrightarrow CO_2(020) + CO_2(020) + HO_2$	1.0×10^{-6}
E31	$H_3O^+ + O_2^- \longrightarrow H_2O + H + O_2$	2.4×10^{-6}
E32	$H_3O^+ + CO_3^- \longrightarrow H_2O + CO_2(020) + OH$	2.4×10^{-6}
E33	$H_3O^+ + CO_4^- \longrightarrow H_2O + CO_2(020) + HO_2$	2.4×10^{-6}
E34	$H_3O^+ + NO_3^- \longrightarrow H_2O + NO_2 + OH$	2.4×10^{-6}
E35	$H_3O^+ + NO_2^- \longrightarrow H_2O + NO_2 + H$	2.4×10^{-6}

Catalytic Species

M_1 = All species

M_2 = All species except O, O_2 and O_3

M_3 = O, O_2, O_3

M_4 = O_2

D45 - Ref. 20; D48, D49, D51 and D53 - Ref. 21. The flame-ion mass spectrometry results of Hurle, Sugden and Nutt (Ref. 22) are the source of coefficient D39. The rate coefficients for the proton transfer reactions D41 and D42 have been estimated to be approximately equal to that for the analogous reaction D40, the rate coefficient for which is that from the drift tube study by Pritchard and Harrison (Ref. 23). Finally, coefficient D46 for the charge transfer reaction between O_2^- and OH has been approximated as the geometric mean of the coefficients for the analogous charge transfer reactions of O_2^- with O_3 and NO_2, i.e., D15 and D16.

- Recombination Reactions

The dissociative ion-free electron recombination coefficients E22, E23 and E24, for HCO^+, HCO_2^+ and H_3O^+, respectively are based on the room temperature results cited in the survey by Biondi (Ref. 12) of the effects of ion complexity on recombination and the following: Coefficient E22, for HCO^+, has been assigned the same ion temperature dependence as coefficient E1, for CO_2^+; Reaction E23, for HCO_2^+, has been estimated simply to be approximately twice as rapid as the corresponding dissociative recombination reaction E1 involving the less complex CO_2^+ ion; Flame temperature results by Calcote et al (Ref. 24) have been combined with the room temperature result cited by Biondi (i.e., $\sim 1 \times 10^{-6}$) to infer a $\sim T^{-0.5}$ ion temperature dependence, which together with the flame results and the generically assumed $u_e^{-0.5}$ dependence leads to coefficient E24.

Ion-ion neutralization coefficients E25 through E35 have all been estimated via the same empirical procedure as developed (see Section 2.2.1) for the generically similar coefficients E4 through E21, viz., scaling by the reduced mass effect of the collision partners and the room temperature assessment of the ion-free electron recombination coefficient of the appropriate positive ion vis a vis that for NO^+.

Excited Species (Table 2): Direct kinetic effects on excited species of the addition of hydrogen are readily and simply incorporated via inclusion

Table 2

EXCITED SPECIES REACTIONS AND RATE COEFFICIENTS[a] FOR THE CO_2 ELECTRIC DISCHARGE LASER

A. Vibrational Pumping Reactions[b]

A1	$N_2(0) + e \longrightarrow N_2(1) + e$	$\dfrac{1.6 \times 10^{-11} \exp(9.1\, u_e)}{1 + 7.0 \times 10^{-4} \exp(9.1\, u_e)}$
A2	$CO(0) + e \longrightarrow CO(1) + e$	$\dfrac{2.4 \times 10^{-7}\, u_e^{0.5} \exp(-1.31/u_e)}{1 + 5.33\, u_e \exp(-1.31/u_e)}$
A3	$CO_2(000) + e \longrightarrow CO_2(001) + e$	$7.9 \times 10^{-9} \exp(-0.38/u_e)$
A4	$CO_2(000) + e \longrightarrow CO_2(010) + e$	$2.0 \times 10^{-8}\, u_e$

B. Electronic Pumping and De-Excitation Reactions[c]

B1	$CO(0) + e \longrightarrow CO^* + e$	$5.3 \times 10^{-9}\, u_e^{0.5} \exp(-2.6/u_e)$
B2	$CO^* + M_1 \longrightarrow CO(0) + M_1$	1.0×10^{-11}
B3	$CO^* + CO_2(000) \longrightarrow CO(0) + O + CO(0)$	1.0×10^{-10}
B4	$N_2(0) + e \longrightarrow N_2^* + e$	$1.3 \times 10^{-5}\, u_e^{-4.6} \exp(-11.5/u_e)$
B5	$N_2^* + M_1 \longrightarrow N_2(0) + M_1$	1.0×10^{-11}
B6	$N_2^* + CO_2(000) \longrightarrow N_2(0) + O + CO(0)$	1.0×10^{-11}
B7	$N_2^* + CO_2(000) \longrightarrow N + NO + CO(0)$	1.0×10^{-10}
B8	$CO_2(000) + e \longrightarrow CO_2^* + e$	$2.5 \times 10^{-9}\, u_e^{1.6} \exp(-5.1/u_e)$
B9	$CO_2^* + M_1 \longrightarrow CO_2(000) + M_1$	1.0×10^{-11}
B10	$CO_2^* + CO_2(000) \longrightarrow CO_2(000) + O + CO(0)$	1.0×10^{-10}

[a] Units are as follows: Rate coefficients, cm^3-particle-sec units; u_e, eV; T, ^oK; R, cal-mole^{-1} $^oK^{-1}$.

[b] All reversible reactions; $k_r = k_f/K$. For the vibrational pumping reactions, K is the equilibrium coefficient for the essentially thermo-neutral forward reaction involving hot electrons.

[c] All forward reactions only.

C. Vibrational Relaxation Reactions[a]

C1	$CO_2(110) + CO_2(000) \longrightarrow CO_2(100) + CO_2(010)$	$1.25 \times 10^{-13}\ T^{0.5}$
C2	$CO_2(030) + CO_2(000) \longrightarrow CO_2(100) + CO_2(010)$	$1.8 \times 10^{-15}\ T^{0.5}$
C3	$CO_2(030) + CO_2(000) \longrightarrow CO_2(020) + CO_2(010)$	$3.1 \times 10^{-13}\ T^{0.5}$
C4	$CO_2(100) + CO_2(000) \longrightarrow CO_2(010) + CO_2(010)$	4.0×10^{-13}
C5	$CO_2(020) + CO_2(000) \longrightarrow CO_2(010) + CO_2(010)$	$1.4 \times 10^{-12}\ T^{0.5}$
C6	$CO_2(001) + M_5 \longrightarrow CO_2(110) + M_5$	$1.1 \times 10^{-27}\ T^{4.8}\ \exp(1484/RT)$
C7	$CO_2(001) + M_8 \longrightarrow CO_2(110) + M_8$	$1.9 \times 10^{-31}\ T^{5.8}\ \exp(2436/RT)$
C8	$CO_2(001) + M_5 \longrightarrow CO_2(030) + M_5$	$8.1 \times 10^{-31}\ T^{5.6}\ \exp(1484/RT)$
C9	$CO_2(001) + M_8 \longrightarrow CO_2(030) + M_8$	$1.4 \times 10^{-34}\ T^{6.6}\ \exp(2436/RT)$
C10	$CO_2(110) + M_6 \longrightarrow CO_2(030) + M_6$	$4.3 \times 10^{-17}\ T^{1.5}$
C11	$CO_2(110) + M_6 \longrightarrow CO_2(020) + M_6$	$4.5 \times 10^{-27}\ T^{4.2}\ \exp(-903/RT)$
C12	$CO_2(110) + M_6 \longrightarrow CO_2(020) + M_6$	$8.8 \times 10^{-20}\ T^{2.5}\ \exp(-4410/RT)$
C13	$CO_2(110) + M_6 \longrightarrow CO_2(100) + M_6$	$8.6 \times 10^{-24}\ T^{3.8}\ \exp(-549/RT)$
C14	$CO_2(030) + M_6 \longrightarrow CO_2(020) + M_6$	$9.3 \times 10^{-22}\ T^{3.3}\ \exp(-1230/RT)$
C15	$CO_2(030) + M_6 \longrightarrow CO_2(100) + M_6$	$1.1 \times 10^{-21}\ T^{3.0}\ \exp(-1060\ RT)$
C16	$CO_2(100) + M_6 \longrightarrow CO_2(020) + M_6$	$8.0 \times 10^{-18}\ T^{1.5}$
C17	$CO_2(100) + M_7 \longrightarrow CO_2(010) + M_7$	$5.6 \times 10^{-22}\ T^{3.3}\ \exp(-1480/RT)$
C18	$CO_2(100) + He \longrightarrow CO_2(010) + He$	$1.8 \times 10^{-21}\ T^{3.0}\ \exp(843/RT)$
C19	$CO_2(100) + CO(0) \longrightarrow CO_2(010) + CO(0)$	$8.4 \times 10^{-10}\ T^{-1.0}$
C20	$CO_2(020) + M_7 \longrightarrow CO_2(010) + M_7$	$2.1 \times 10^{-21}\ T^{3.2}\ \exp(-1350/RT)$
C21	$CO_2(020) + He \longrightarrow CO_2(010) + He$	$3.8 \times 10^{-21}\ T^{3.0}\ \exp(843/RT)$
C22	$CO_2(020) + CO(0) \longrightarrow CO_2(101) + CO(0)$	$1.7 \times 10^{-9}\ T^{-1.0}$

[a] All reversible reactions.

C23	$CO_2(010) + M_7 \longrightarrow CO_2(000) + M_7$	$3.4 \times 10^{-26}\ T^{4.2}\ \exp(1130/RT)$
C24	$CO_2(010) + He \longrightarrow CO_2(000) + He$	$9.9 \times 10^{-22}\ T^{3.0}\ \exp(843/RT)$
C25	$CO_2(010) + CO(0) \longrightarrow CO_2(000) + CO(0)$	$4.5 \times 10^{-10}\ T^{-1.0}$
C26	$CO_2(001) + N_2(0) \longrightarrow CO_2(000) + N_2(1)$	$8.3 \times 10^{-12}\ T^{-0.5}$
C27	$CO_2(001) + CO(0) \longrightarrow CO_2(000) + CO(1)$	$1.4 \times 10^{-17}\ T^{1.65}$
C28	$N_2(1) + CO(0) \longrightarrow N_2(0) + CO(1)$	$2.7 \times 10^{-18}\ T^{1.5}$
C29	$CO_2(010) + H_2O \longrightarrow CO_2(000) + H_2O$	$3.2 \times 10^{-13}\ \exp(22.9/T^{1/3})$
C30	$CO_2(001) + H_2O \longrightarrow CO_2(030) + H_2O$	4.0×10^{-13}
C31	$N_2(1) + H_2O \longrightarrow N_2(0) + H_2O$	$1.1 \times 10^{-10}\ \exp(-68.9/T^{1/3})$
C32	$CO(1) + H_2O \longrightarrow CO(0) + H_2O$	$3.1 \times 10^{-10}\ \exp(-65.0/T^{1/3})$
C33	$CO_2(010) + H_2 \longrightarrow CO_2(000) + H_2$	3.0×10^{-12}
C34	$CO_2(001) + H_2 \longrightarrow CO_2(110) + H_2$	$1.7 \times 10^{-17}\ T^{1.5}$

Catalytic Species

M_1 = All species

M_5 = All species except He and N_2

M_6 = 1.5 He; All others: 1.0

M_7 = 0.5 N_2; CO = He = 0; All others: 1.0

M_8 = He, $2N_2$

of the dominant relaxation rates of the upper and lower laser levels of CO_2 by H_2, Reactions C33 and C34. Rate coefficients C33 and C34 are the result of curve fits to the recent data survey and theoretical evaluations by Stricker (Ref. 25).

Free Radical Species (Table 3): For the most part the additional reactions and rate coefficients required to extend the CO_2-CO-N_2-He free radical species hinetics given in Ref. 2 to combustion gas mixtures (i.e., Reactions A8 through A17 and B14 through B36) have been taken directly from the current Lockheed LAMP reaction models used fairly extensively for analysis of chemical lasers and rocket exhaust plumes*. The few exceptions are discussed below.

- Ternary Recombination Reactions. The ternary rate coefficient for Reaction A14 leading to HNO_3 is that adopted in the theoretical stratospheric model developed by Shimazaki and Ogawa (Ref. 27). Reactions A15, A16 and A17 are normally ternary in stratospheric applications (see, e.g., Ref. 28). At pressures on the order of atmospheric, however, they follow essentially binary behavior, being at their high pressure limit (Ref. 29). Coefficients A15, A16 and A17 are the recommended survey values given by Baulch et al., (Ref. 29) for these rate coefficients in their binary limit.

- Binary Reactions. Rate coefficient B19 for the $H+NO_2$ reaction is the recommended survey value given by Baulch et al., (Ref. 29). Coefficients B17, B22, B23, B24, B27 and B30 are those adopted by Wuebbles and Chang (Ref. 30) in their study of the temporal behavior of the stratospheric distribution of minor chemical constituents. Coefficient B16 for the reaction between OH and HNO_2 has been estimated as approximately equal to that for the analogous reaction, B17, between OH and HNO_3.

*These models are kept as current as possible by incorporation of recent results as these are made available, the most recent documentation being Ref. 26. Validation via correlation with data has largely been successful.

Table 3

FREE RADICAL SPECIES REACTIONS[a] AND RATE COEFFICIENTS[b] FOR THE CO_2 ELECTRIC DISCHARGE LASER

A. Ternary Recombination Reactions		Rate Coefficients
A1	$N + N + M_9 \longrightarrow N_2(1) + M_9$	$8.3 \times 10^{-34} \exp(1000/RT)$
A2	$N + O + M_9 \longrightarrow NO + M_9$	$1.8 \times 10^{-31} T^{-0.5}$
A3	$O + CO(0) + M_{10} \longrightarrow CO_2(020) + M_{10}$	$2.0 \times 10^{-33} \exp-(4000/RT)$
A4	$O + O + M_9 \longrightarrow O_2 + M_9$	$3.8 \times 10^{-30} T^{-1} \exp-(340/RT)$
A5	$O + O_2 + M_9 \longrightarrow O_3 + M_9$	$1.0 \times 10^{-34} \exp(1010/RT)$
A6	$O + NO + M_9 \longrightarrow NO_2 + M_9$	$4.0 \times 10^{-33} \exp(1880/RT)$
A7	$O + NO_2 + M_9 \longrightarrow NO_3 + M_9$	$1.8 \times 10^{-32} \exp(1000/RT)$
A8	$H + H + M_9 \longrightarrow H_2 + M_9$	$2.8 \times 10^{-30} T^{-1.0}$
A9	$O + H + M_9 \longrightarrow OH + M_9$	1.0×10^{-32}
A10	$H + OH + M_9 \longrightarrow H_2O + M_9$	$6.1 \times 10^{-26} T^{-2.0}$
A11	$H + O_2 + M_9 \longrightarrow HO_2 + M_9$	$2.1 \times 10^{-32} \exp(580/RT)$
A12	$CHO + M_9 \longrightarrow CO(0) + H + M_9$	$1.2 \times 10^{-10} \exp(-15000/RT)$
A13	$CH_2O + M_9 \longrightarrow CO(0) + H_2 + M_9$	$3.5 \times 10^{-8} \exp(-35000/RT)$
A14	$HO_2 + NO + M_9 \longrightarrow HNO_3 + M_1$	3.5×10^{-31}
A15	$OH + NO_2 \longrightarrow HNO_3$	$1.0 \times 10^{-11} \exp(-340/RT)$
A16	$OH + NO \longrightarrow HNO_2$	2.0×10^{-12}
A17	$NO_2 + NO_3 \longrightarrow N_2O_5$	4.0×10^{-12}

[a] All reversible reactions.

[b] Units are as follows: Rate coefficients, cm^3-particle-sec units; T, ^oK; R, cal-$mole^{-1}$-$^oK^{-1}$.

B. Binary Reactions

B1	$N + NO \longrightarrow N_2(0) + O$	2.7×10^{-11}
B2	$N + NO_2 \longrightarrow NO + NO$	1.4×10^{-12}
B3	$N + NO_3 \longrightarrow NO + NO_2$	5.7×10^{-13}
B4	$N + O_2 \longrightarrow NO + O$	$1.1 \times 10^{-14}\ T\ \exp(-6300/RT)$
B5	$N + O_3 \longrightarrow NO + O_2$	5.7×10^{-13}
B6	$O + O_3 \longrightarrow O_2 + O_2$	$1.9 \times 10^{-11}\ \exp(-4600/RT)$
B7	$O + NO_2 \longrightarrow O_2 + NO$	$1.6 \times 10^{-10}\ T^{-0.5}$
B8	$O + NO_3 \longrightarrow O_2 + NO_2$	5.7×10^{-13}
B9	$NO + NO_3 \longrightarrow NO_2 + NO_2$	8.7×10^{-12}
B10	$NO + O_3 \longrightarrow NO_2 + O_2$	$9.0 \times 10^{-13}\ \exp(-2400/RT)$
B11	$NO_2 + O_3 \longrightarrow NO_3 + O_2$	$1.2 \times 10^{-13}\ \exp(-4900/RT)$
B12	$NO_2 + NO_3 \longrightarrow NO_2 + O_2 + NO$	$2.3 \times 10^{-13}\ \exp(-3200/RT)$
B13	$NO_3 + NO_3 \longrightarrow NO_2 + O_2 + NO_2$	$5.0 \times 10^{-12}\ \exp(-6000/RT)$
B14	$OH + CO(0) \longrightarrow CO_2(000) + H$	$1.1 \times 10^{-19}\ T^2\ \exp(1600/RT)$
B15	$OH + H_2 \longrightarrow H_2O + H$	$1.0 \times 10^{-17}\ T^2\ \exp(-2900/RT)$
B16	$OH + HNO_2 \longrightarrow H_2O + NO_2$	$3.5 \times 10^{-13}\ \exp(-600/RT)$
B17	$OH + HNO_3 \longrightarrow H_2O + NO_3$	$3.5 \times 10^{-13}\ \exp(-600/RT)$
B18	$OH + N \longrightarrow NO + H$	5.3×10^{-11}
B19	$H + NO_2 \longrightarrow OH + NO$	$6.0 \times 10^{-10}\ \exp(-1500/RT)$
B20	$OH + O \longrightarrow H + O_2$	4.0×10^{-11}
B21	$OH + OH \longrightarrow H_2O + O$	$1.0 \times 10^{-11}\ \exp(-1100/RT)$
B22	$H + O_3 \longrightarrow OH + O_2$	2.6×10^{-11}
B23	$OH + O_3 \longrightarrow HO_2 + O_2$	$1.6 \times 10^{-12}\ \exp(-2000/RT)$

B24	$O + N_2O_5 \longrightarrow NO_2 + NO_2 + O_2$	1.0×10^{-14}
B25	$HO_2 + H \longrightarrow OH + OH$	4.2×10^{-10} exp(-1900/RT)
B26	$HO_2 + H \longrightarrow H_2 + O_2$	4.2×10^{-11} exp(-700/RT)
B27	$HO_2 + NO \longrightarrow NO_2 + OH$	2.0×10^{-13}
B28	$HO_2 + O \longrightarrow OH + O_2$	8.0×10^{-11} exp(-1000/RT)
B29	$HO_2 + OH \longrightarrow H_2O + O_2$	8.3×10^{-11} exp(-1000/RT)
B30	$HO_2 + O_3 \longrightarrow OH + O_2 + O_2$	1.0×10^{-13} exp(-2500/RT)
B31	$CH_2O + H \longrightarrow CHO + H_2$	2.2×10^{-11} exp(-3800/RT)
B32	$CH_2O + O \longrightarrow CHO + OH$	1.6×10^{-13}
B33	$CH_2O + OH \longrightarrow CHO + H_2O$	9.0×10^{-13} $T^{0.5}$
B34	$CHO + O \longrightarrow CO(0) + OH$	2.1×10^{-10}
B35	$CHO + OH \longrightarrow CO(0) + H_2O$	2.1×10^{-10}
B36	$CHO + O_2 \longrightarrow CO(0) + HO_2$	8.3×10^{-11} exp(-1600/RT)

Catalytic Species

M_9 = 2 CO_2, He; All others: 1.0

M_{10} = 3 CO_2, 1.5 CO; 20 O_2; All others: 1.0

Section 3
RESULTS

3.1 COMPARISON WITH EXPERIMENT

In order to put results and possible recommendations derived from the theoretical model discussed in Section 2 into perspective it was felt desirable to first test and validate the model against some available experimental data. Suitable results for comparison were found in a paper by Dezenberg, Cason and Huff (Ref. 31) which presents single pulse performance data for an electron beam-sustained electric discharge laser. These data have the additional advantage that they were obtained using the standard $CO_2/N_2/He = 1/2/3$ mixture which was previously analyzed by the present authors in connection with a study of a continuous wave electron beam-sustained laser (Refs. 1, 2). The first theoretical results obtained in the present study pertain to the case of 5 atm initial cavity pressure as discussed in Ref. 31. The E/p value of 3.5 kV cm^{-1} atm^{-1} as reported there then implies an electric field strength of 17.5 kV/cm, and – using the given electrode separation of 4 cm – an applied drift field potential of 70 kV. Unsaturated gain measurements were made using a nominal post-foil electron beam current density equal to 220 mA/cm^2, which was also used in the present calculations. Oscillator performance calculations with the present model considered optical cavity data as indicated in Refs. 31 and 32 using an 8% reflectivity for the Na Cℓ output flat (Ref. 33). Theoretical results for this case are summarized and compared with experiment in Figs. 1 through 4 and Table 4. Figure 1 shows the temporal behavior of the post-foil electron beam current density assumed in our calculations, while Fig. 2 shows the drift field voltage as observed in the experiment and as used in our calculations. The pulse width used in the calculations was set at 1.6 μsec as indicated by the sharp drop in the experimentally observed distributions of gun current (see Ref. 31) and drift field voltage at that time. While the present calculations assume an instantaneous cutoff in both electron beam current density and drift field voltage, the experiment shows a finite rate of decay at least for the latter, indicating the possibility of some pumping

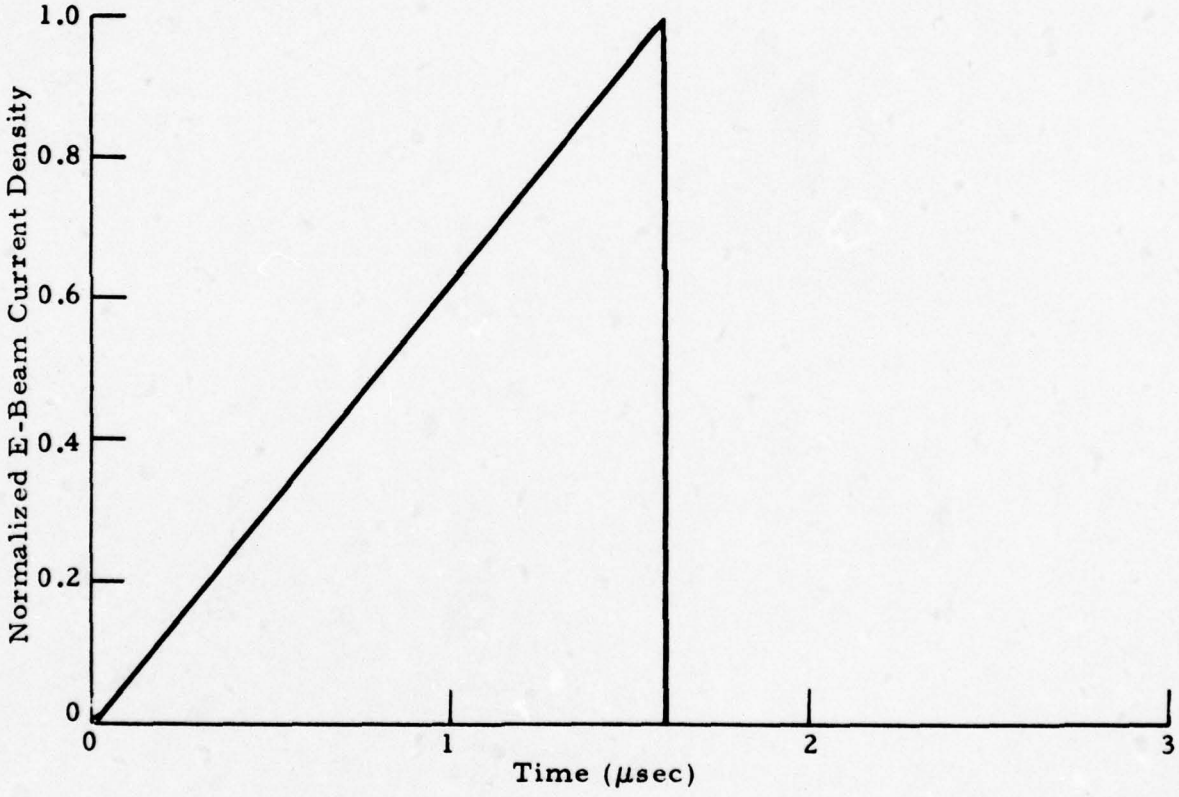

Fig. 1 - Temporal Behavior of Post-Foil Electron-Beam Current Density at 5 atm (Peak Value Corresponds to 220 mA/cm^2)

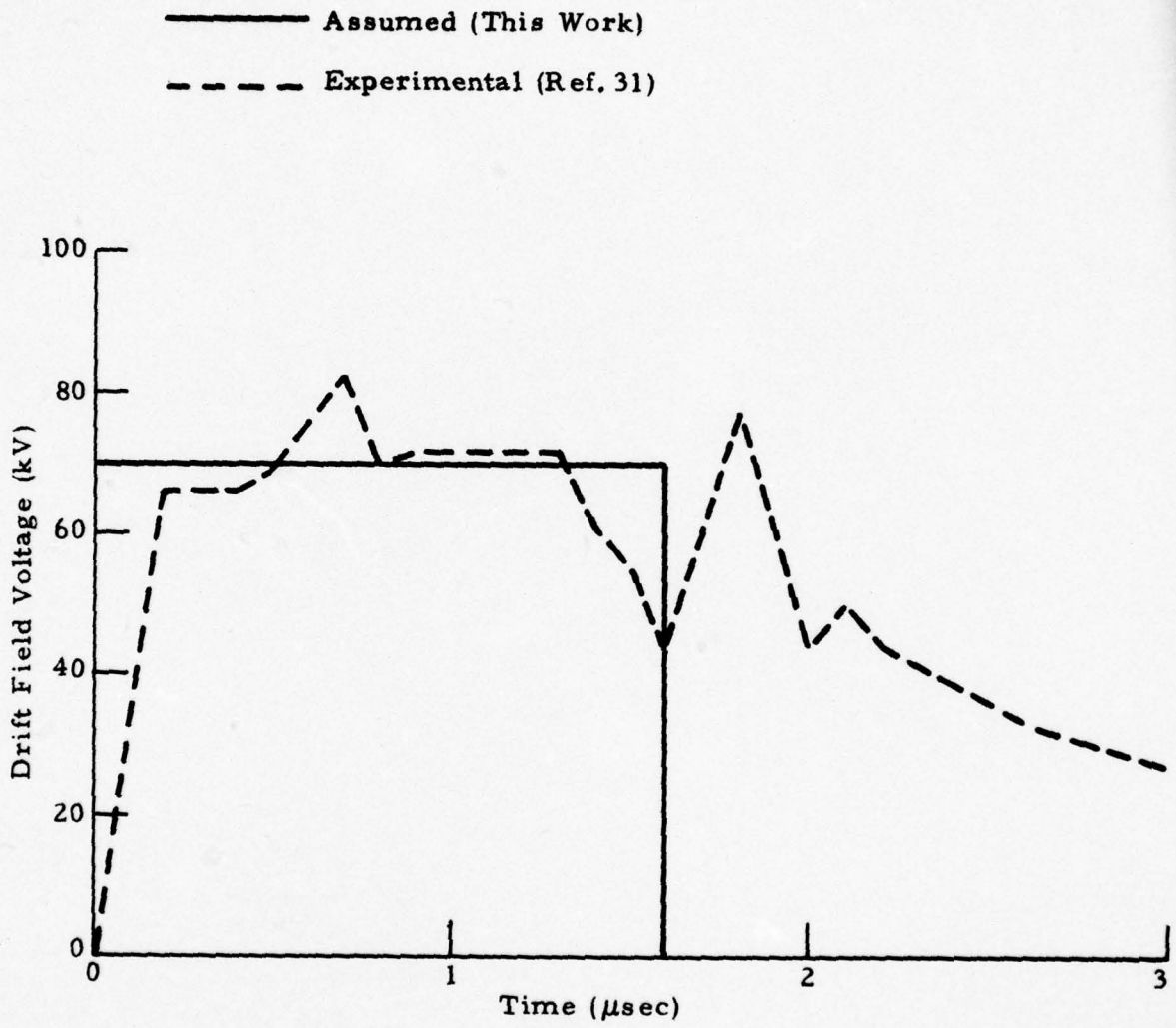

Fig. 2 - Temporal Behavior of Drift Field Voltage at 5 atm

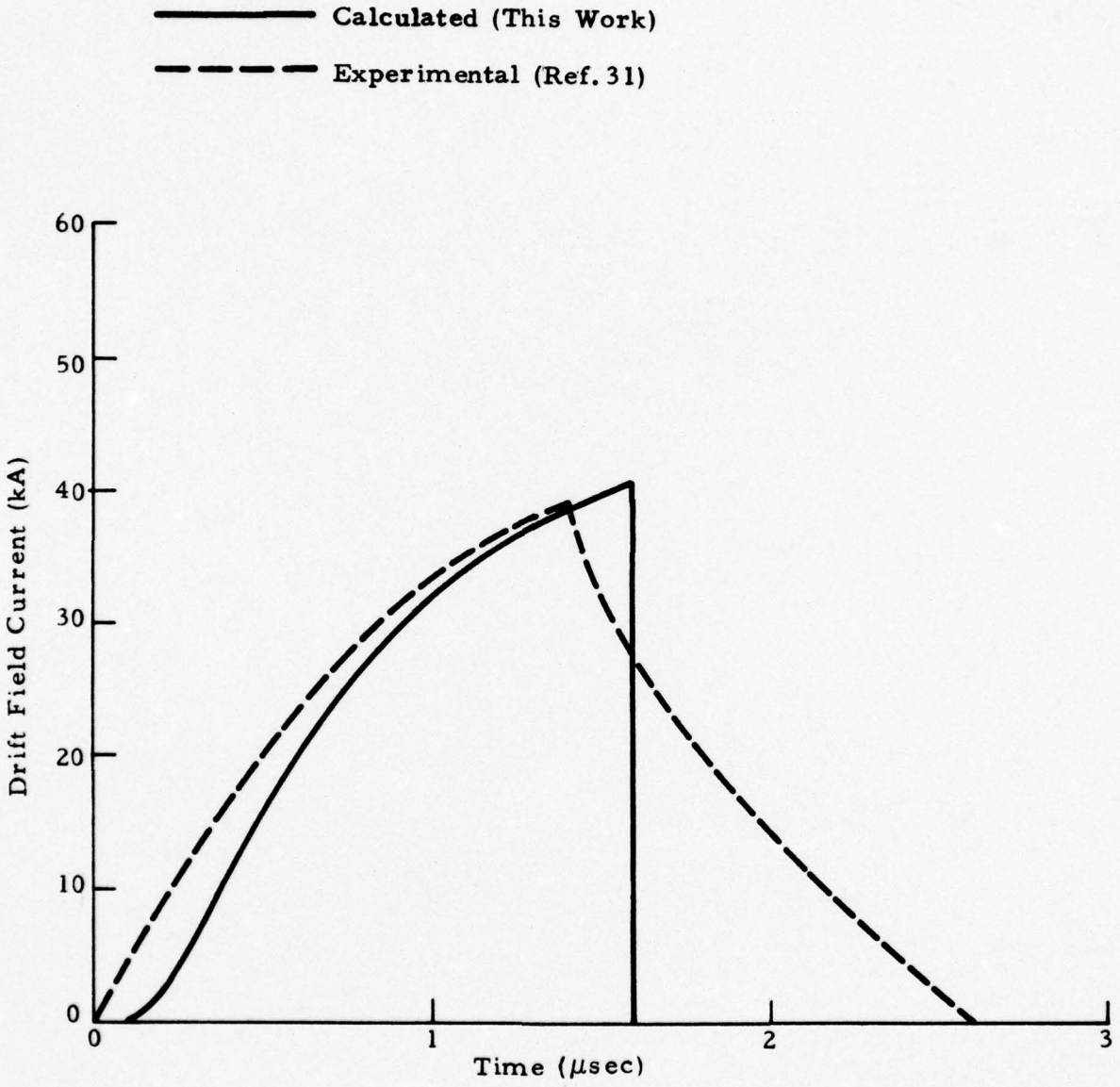

Fig. 3 - Temporal Behavior of Drift Field Current at 5 atm

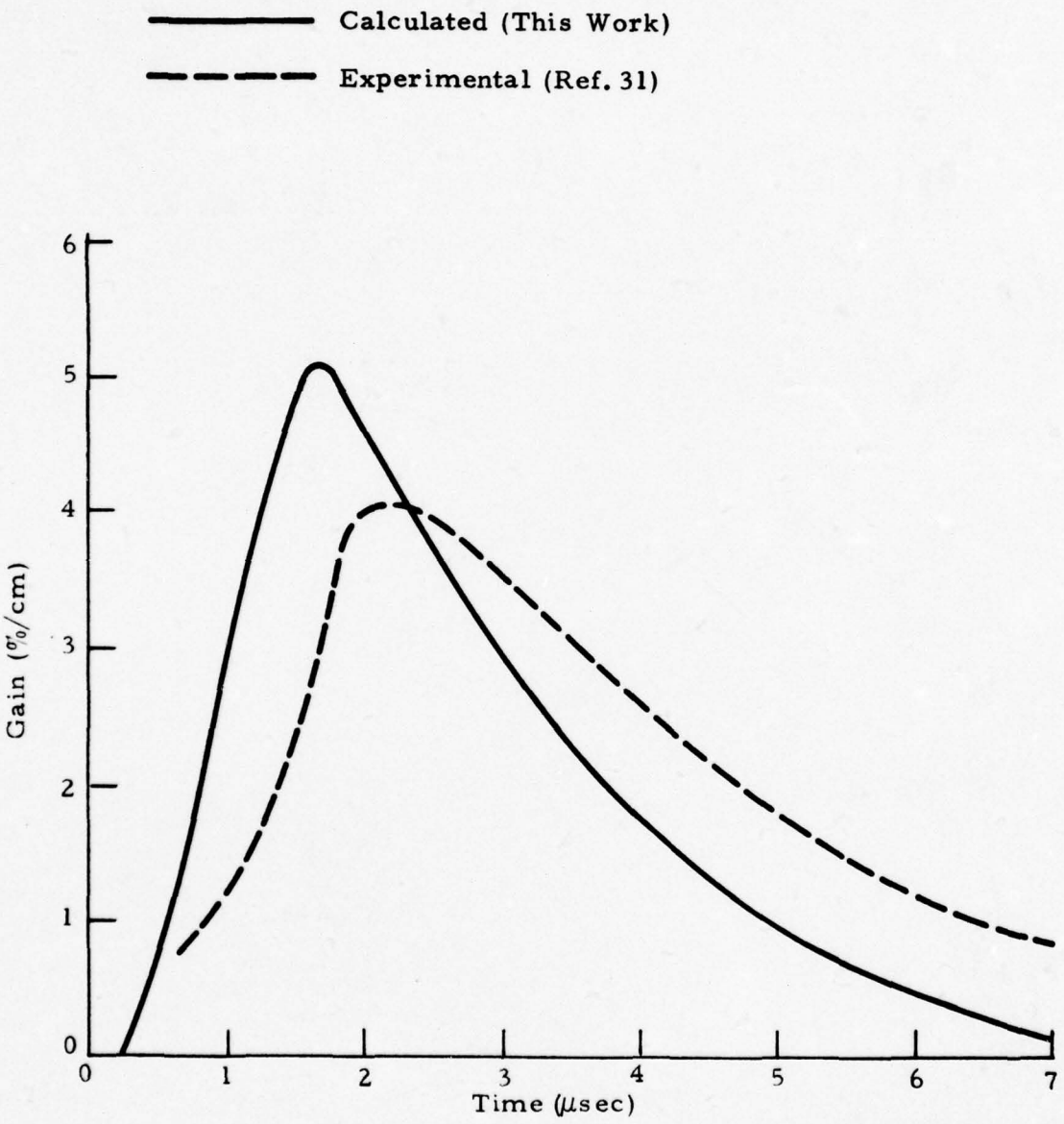

Fig. 4 - Temporal Behavior of Unsaturated Gain at 5 atm

Table 4

PERFORMANCE COMPARISON

	Theory (This Work)	Experiment (Ref. 31)
Initial Pressure (atm)	5.0	5.0
Cavity Volume (lit)	4.0	4.0
Drift Field (kV/cm-atm)	3.5	3.67
Output Energy Density (J/lit-atm)	10.2	12.5
Pulse Energy (J/pulse)	204	250

beyond the nominal duration of the pulse. Further evidence for this is seen in the temporal behavior of the resulting drift field current shown in Fig. 3. While the agreement between theory and experiment is excellent over the major part of the pulse width, the calculated drift field current vanishes at the end of the pulse simply as a result of the vanishing drift field potential. Unsaturated gain distributions as measured and as calculated are compared in Fig. 4. It is interesting to note that Dezenberg, Cason and Huff state in their paper that gain coefficients in excess of 5% cm^{-1} were obtained at 5 atm, just as predicted by the present calculations. Overall, the agreement of measured and calculated temporal behavior of the unsaturated gain is considered very satisfactory.

Finally, calculated laser output energy is compared with experimental data as shown in Table 4. Although the experimental drift field strength of 3.67 kV/cm-atm at otherwise unchanged conditions indicates a discharge voltage slightly higher than 70 kV, the theoretical results are, for simplicity, based on the previously mentioned conditions (i.e., 3.5 kV/cm-atm). Both theoretical output energy density and pulse energy are approximately 18% lower than their measured counterparts. Considering the functional relationship between power input and E/p only (see Eq. (16)), a roughly 15% lower value for the calculated laser output would be expected if it can be assumed that efficiency is unaffected. Considering in addition the differences in

post-pulse temporal behavior of electron-beam current and drift field voltage, the difference between theory and experiment appears entirely accounted for. It can therefore be concluded that theory and experiment are basically in agreement.

3.2 SINGLE PULSE BEHAVIOR OF SEVERAL GAS MIXTURES

Using identical electric discharge conditions an investigation was made of the theoretical single pulse performance of two mixtures containing hydrogen in order to compare with the standard $CO_2/N_2/He = 1/2/3$ mixture. The first mixture was of clean $CO_2/N_2/H_2 = 1/3/0.1$ composition while the second mixture was representative of a laser gas that could conceivably be obtained by hydrocarbon combustion, namely $CO_2/CO/N_2/H_2 = 1/0.25/5.5/0.125$ including 0.15% of O_2 and CH_2O each, as well as 0.015% NO (Ref. 18).

For all the gases, initial conditions in the laser cavity were assumed to be 200 K and 1 atm. Post-foil electron beam current density and effective beam electron energy were set at 100 mA/cm^2 and 100 keV, respectively. The applied discharge potential was assumed to be 25 kV across the 5 cm gap between the discharge electrodes, resulting in an electric field of 5 kV/cm and an E/N value of $1.36 \cdot 10^{-16}$ V cm^2. Pulse widths for the electron beam and the discharge were 8 μsec and 10 μsec, respectively, both being initiated simultaneously. Only square pulses were investigated. Discharge electrode dimensions were assumed to be 5 x 25 cm, resulting in a discharge volume of 0.625 liters. The conditions assumed are representative for the small scale circulator planned by the Army (Ref. 34).

Calculated drift field current density distributions are shown in Fig. 5. Corresponding values for the total drift field energy input are 590, 510 and 755 J lit^{-1} atm^{-1} for the three mixtures $CO_2/N_2/He$, $CO_2/N_2/H_2$ and $CO_2/CO/N_2/H_2$, respectively. Temporal behavior of the secondary electron energy, of the gas temperature and the unsaturated gain are shown in Figs. 6, 7 and 8, respectively. It is interesting to note that the gain begins to decay in all three gas mixtures as soon as the temperature exceeds about 350 K.

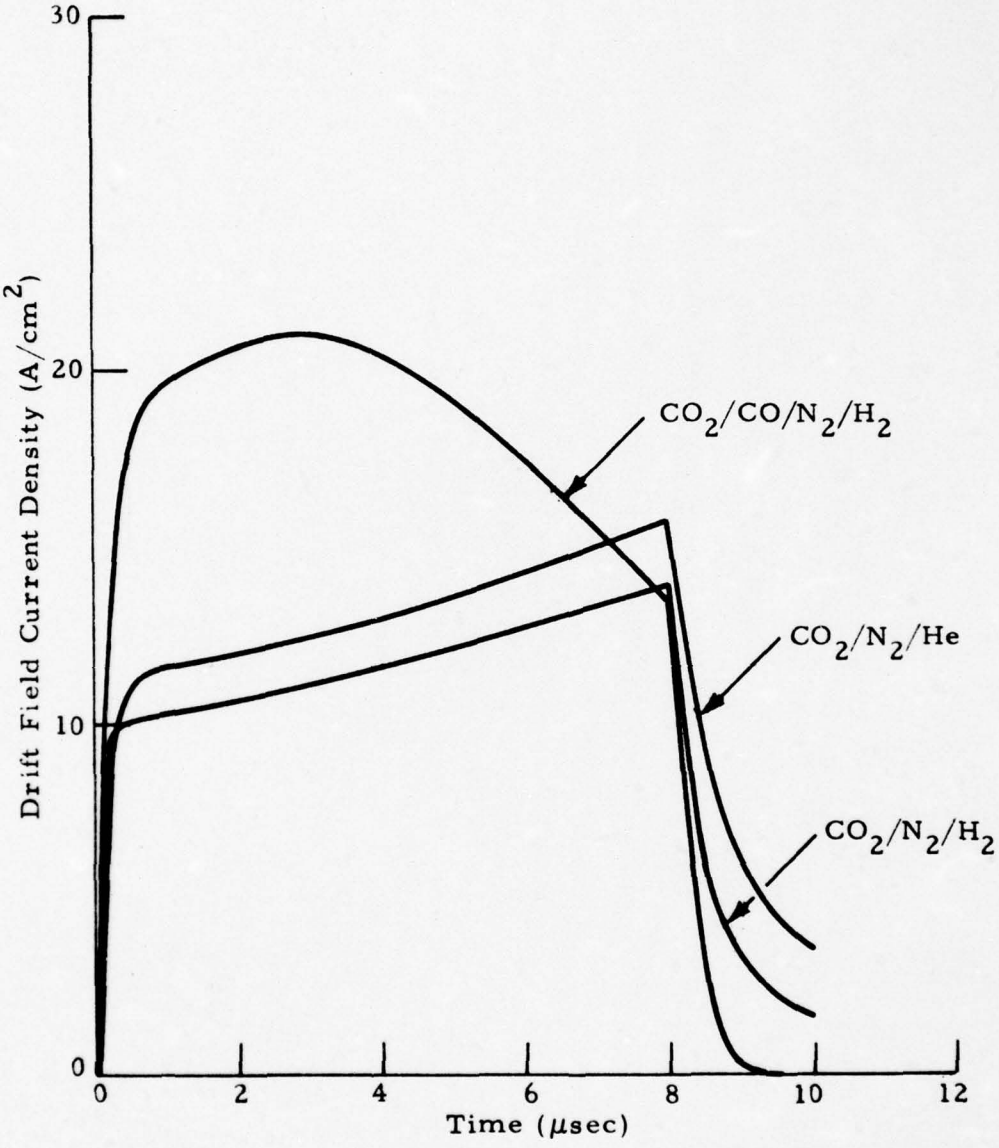

Fig. 5 - Predicted Single Pulse Temporal Behavior of Drift Field Current Density

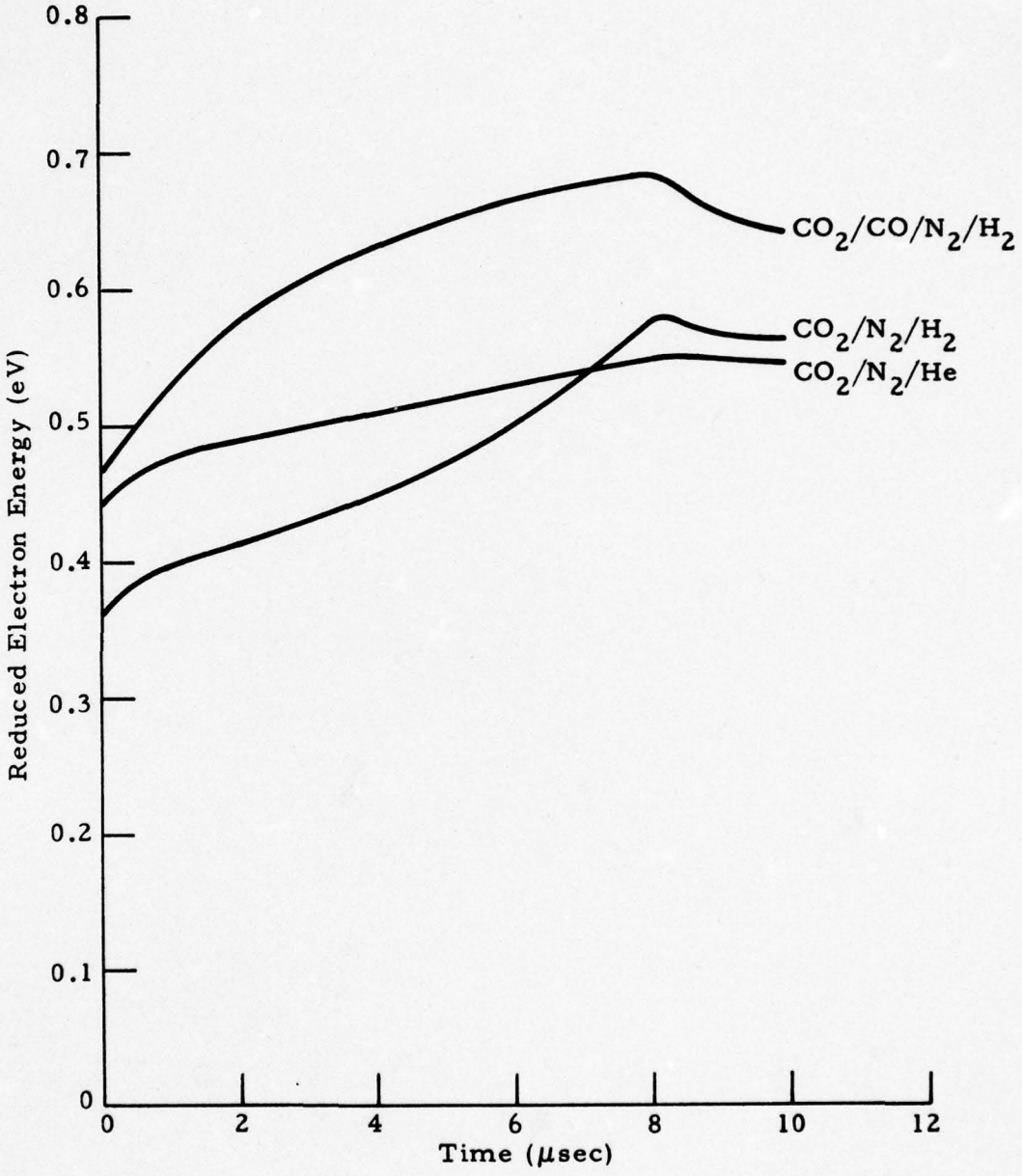

Fig. 6 - Predicted Single Pulse Temporal Behavior of Secondary Electron Energy

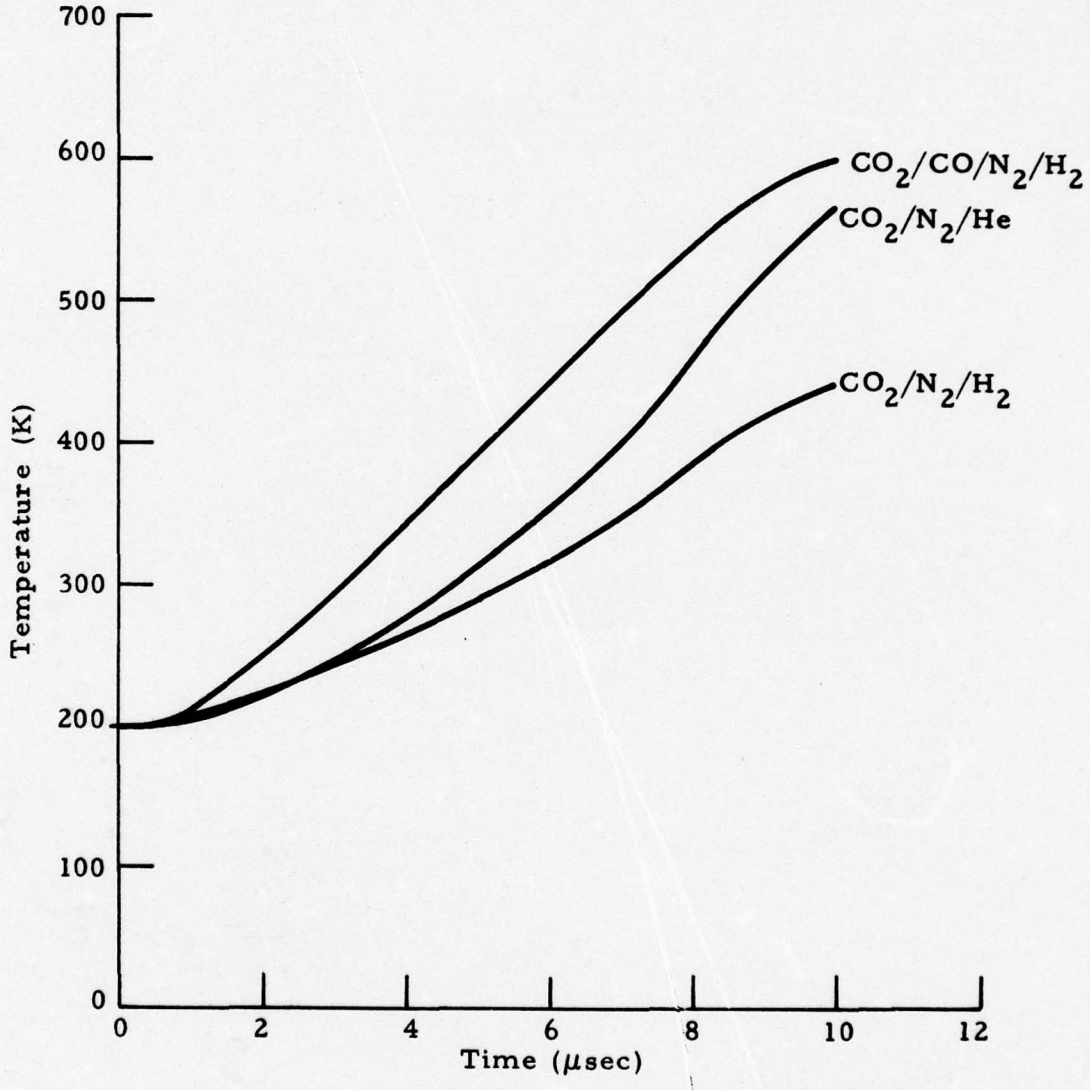

Fig. 7 - Predicted Single Pulse Temporal Behavior of Gas Temperature

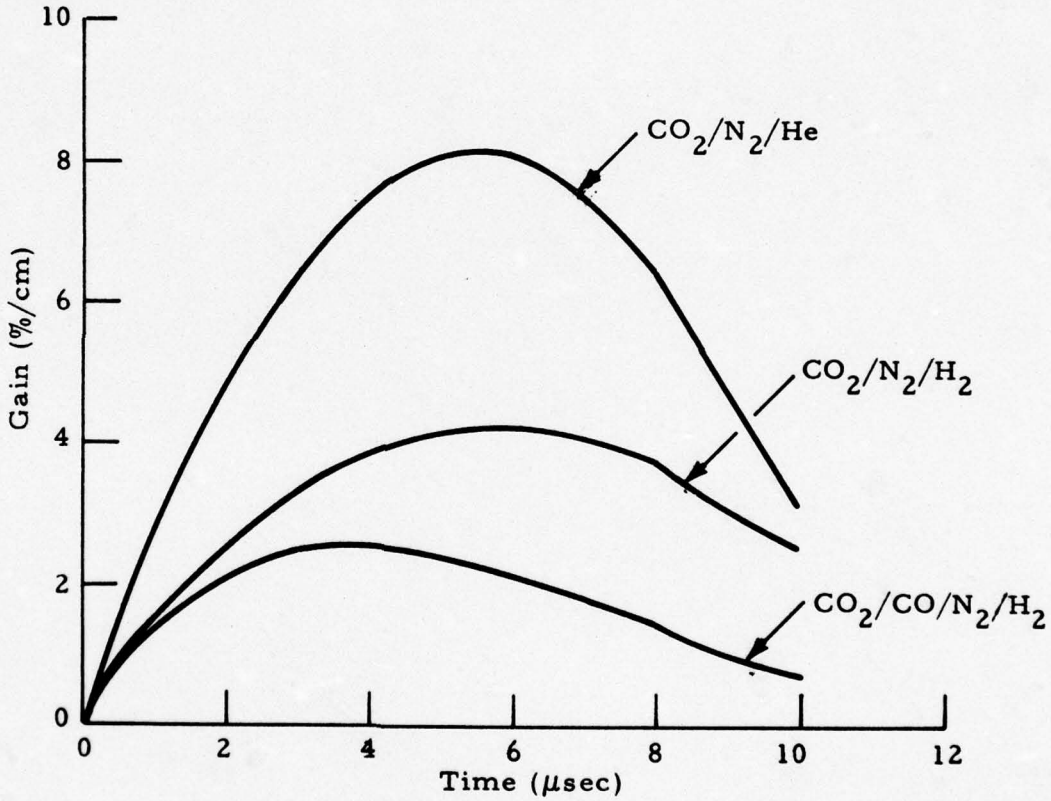

Fig. 8 - Predicted Single Pulse Temporal Behavior of Unsaturated Gain Coefficient

Plasma chemistry effects in the three gas mixtures are shown in Figs. 9, 10 and 11 in terms of temporal distributions of the major species being formed in the discharge. Figure 9 displays results for the $CO_2/N_2/He$ mixture, with neutral species being shown in Fig. 9a, electrons and negative ions in Fig. 9b, and positive ions in Fig. 9c. For the $CO_2/N_2/He$ mixture, the major electrophilic species to be expected are O_3 and NO_2. In a single pulse discharge only the latter is being formed in any noticeable amount as seen in Fig. 9a, and at this level NO_2 apparently has no appreciable effect on the free electron concentration shown in Fig. 9b. The dominant neutral species formed in the discharge are atomic oxygen, carbon monoxide, plus atomic nitrogen and nitric oxide in equal amounts. A very small amount of oxygen and nitrogen dioxide is also predicted. The dominant ions formed are CO_3^- and CO_2^+, as seen from Figs. 9b and 9c. Note that CO_2^+, its distribution practically paralleling that of the free electrons, almost entirely accounts for overall charge neutrality in the plasma.

Plasma chemistry results for the $CO_2/N_2/H_2$ mixture are shown in Fig. 10. As seen in Fig. 10a, atomic hydrogen now is by far the dominant neutral species being generated in the discharge. CHO, N, NO and O all reach levels of a few parts per million at the end of the discharge, and everything else is formed only in even smaller amounts. The formation of NO_2 barely reaches the one part per billion level at the end of the discharge. Thus, just as for the $CO_2/N_2/He$ mixture discussed previously, the essential absence of major electrophilic species during the first pulse results in a steady increase of the free electron density and the drift field current density as shown in Figs. 10b and 5, respectively, until the electron beam pulse terminates at 8 μsec. CO_3^- is again the most prominant negative ion, however, HCO_2^+ now is the dominant positive ion with CO_2^+ at a level approximately two orders of magnitude lower (see Figs. 10b and 10c).

It is important to realize that, of course, the formation of no species can be predicted in the type of calculations being discussed here unless it is provided for in the set of reactions. Theoretical results like these therefore

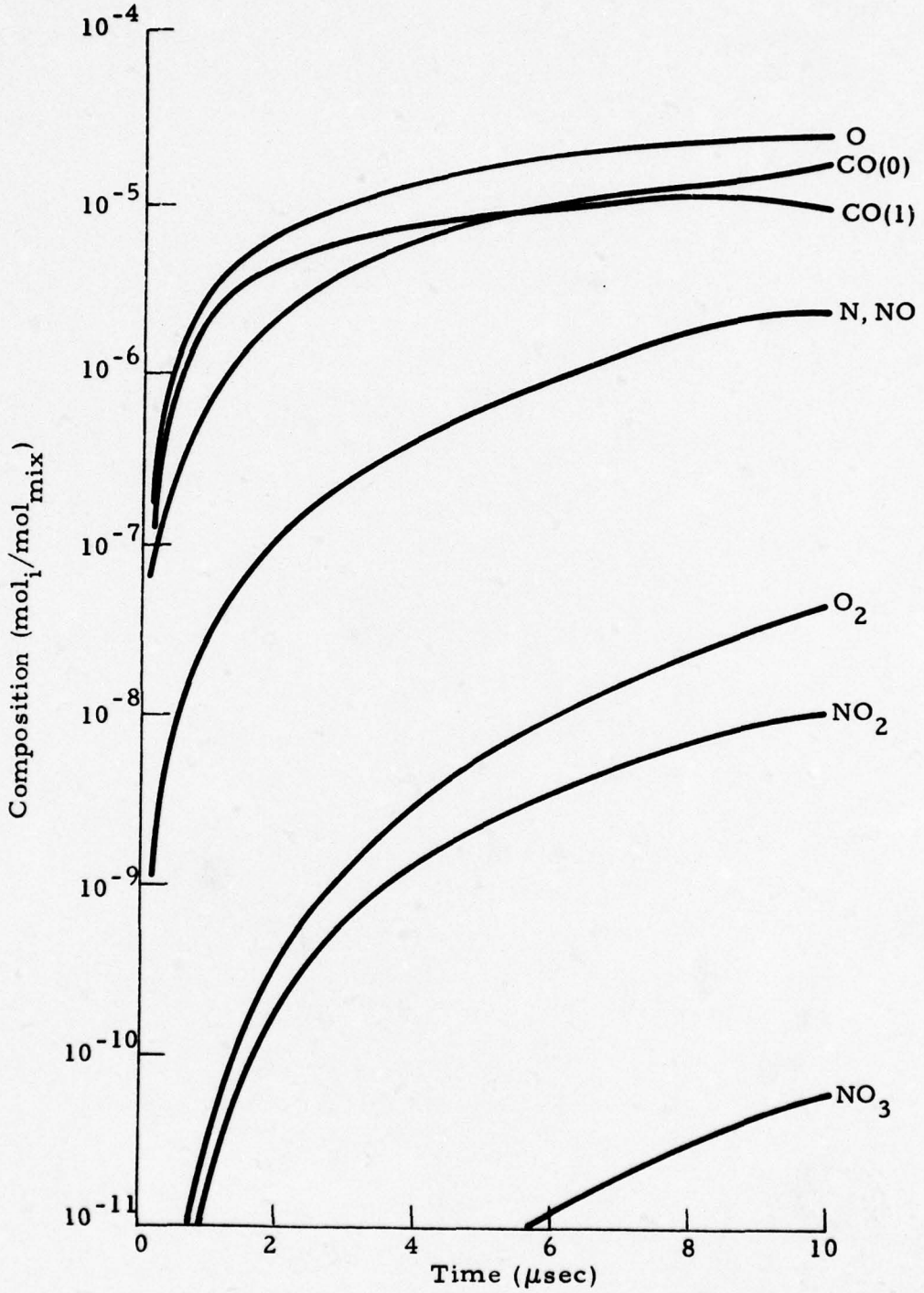

Fig. 9a - $CO_2/N_2/He$ = 1/2/3; Predicted Single Pulse Temporal Behavior of Major Discharge-Generated Neutral Species

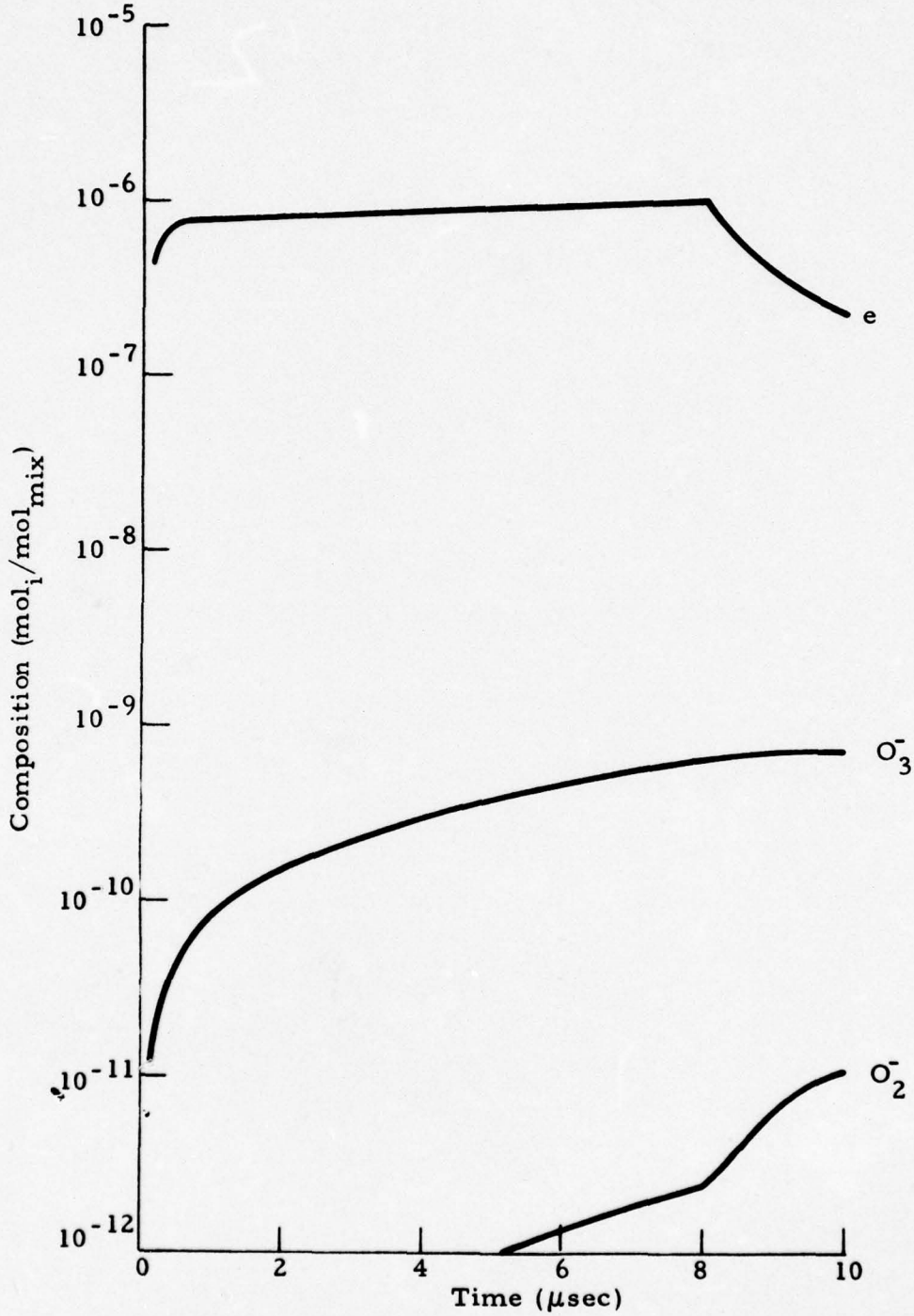

Fig. 9b - $CO_2/N_2/He$ = 1/2/3; Predicted Single Pulse Temporal Behavior of Major Discharge-Generated Negatively Charged Species

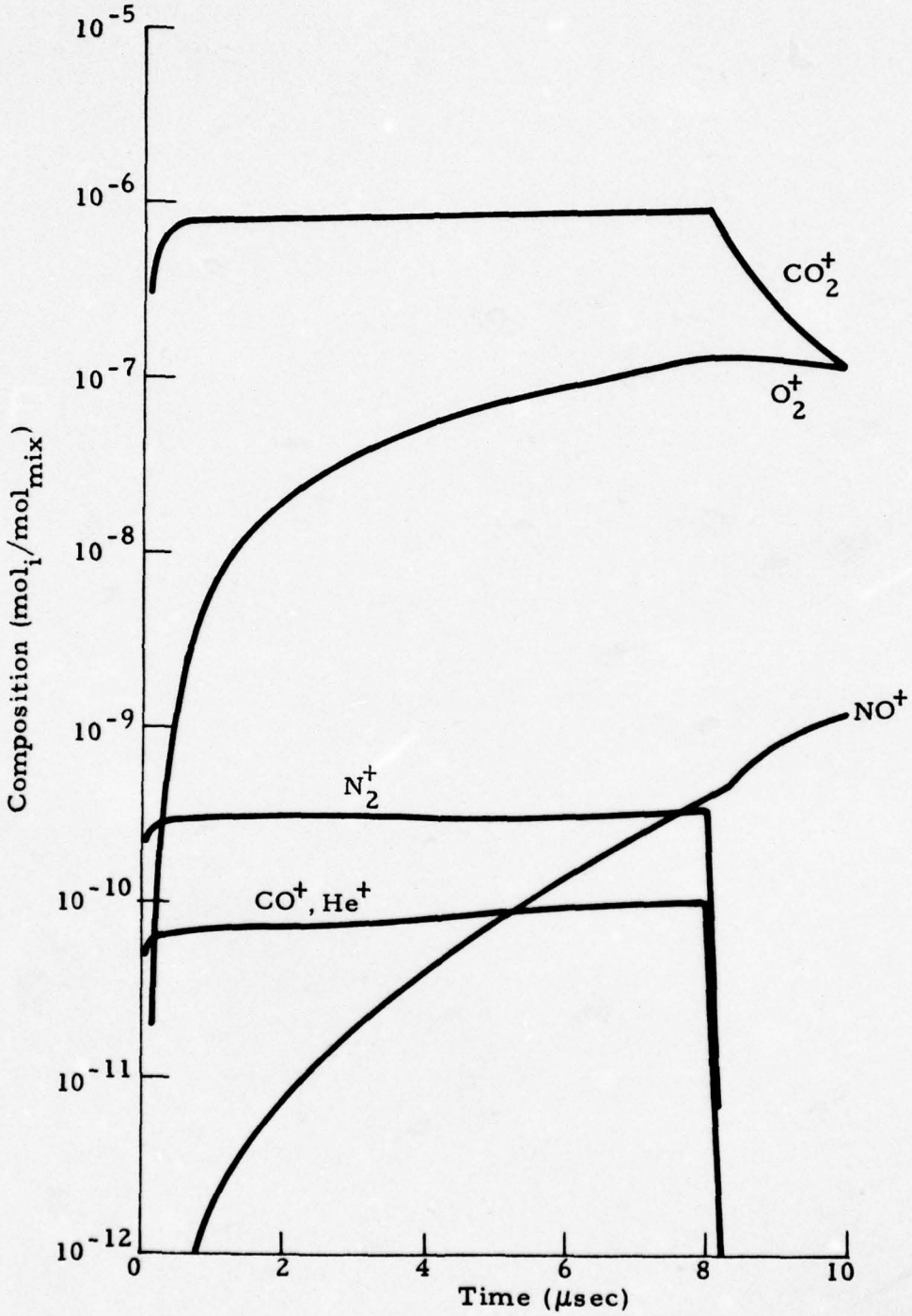

Fig. 9c - $CO_2/N_2/He$ = 1/2/3; Predicted Single Pulse Temporal Behavior of Major Discharge-Generated Positively Charged Species

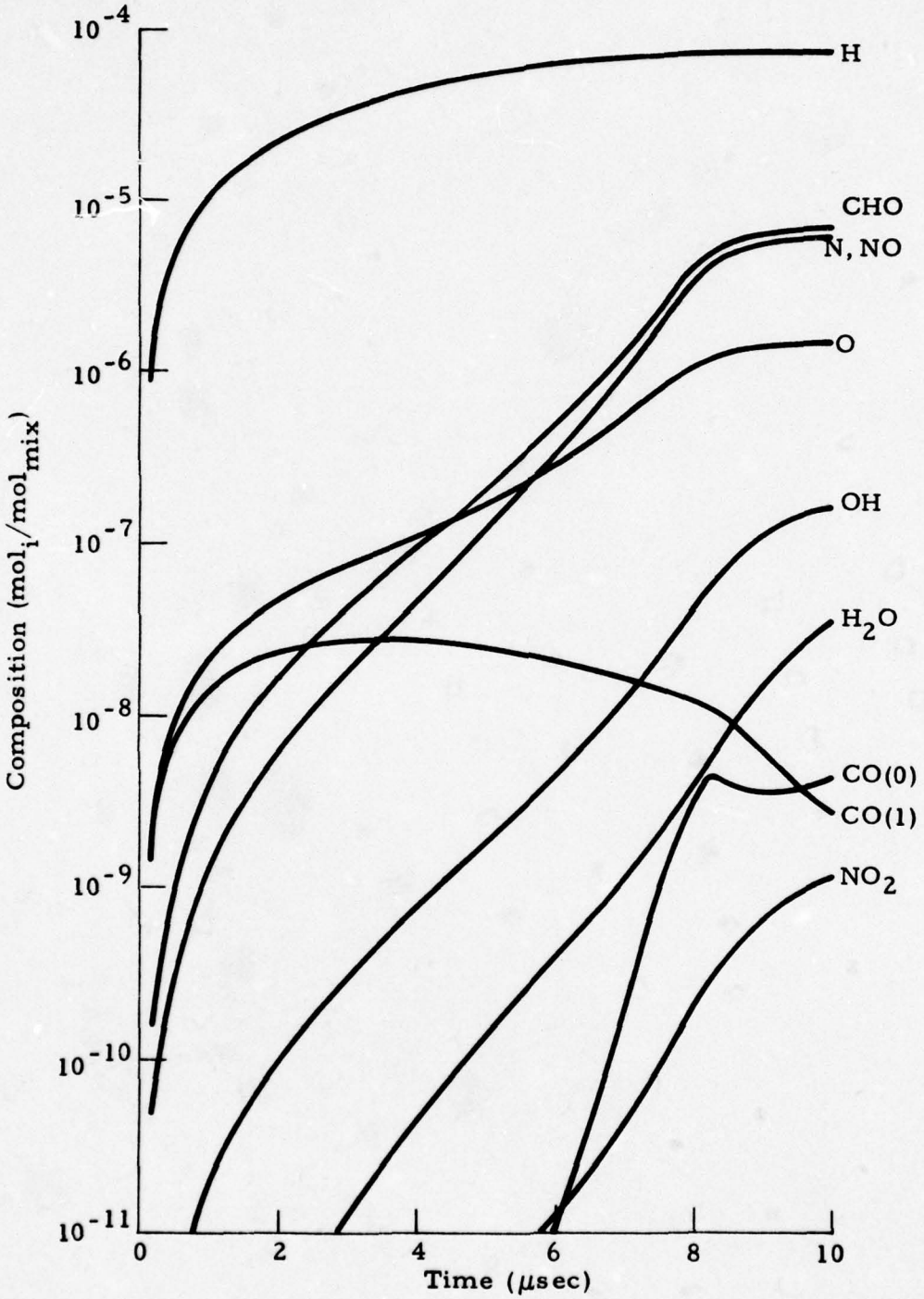

Fig. 10a - $CO_2/N_2/H_2$ = 1/3/0.1; Predicted Single Pulse Temporal Behavior of Major Discharge-Generated Neutral Species

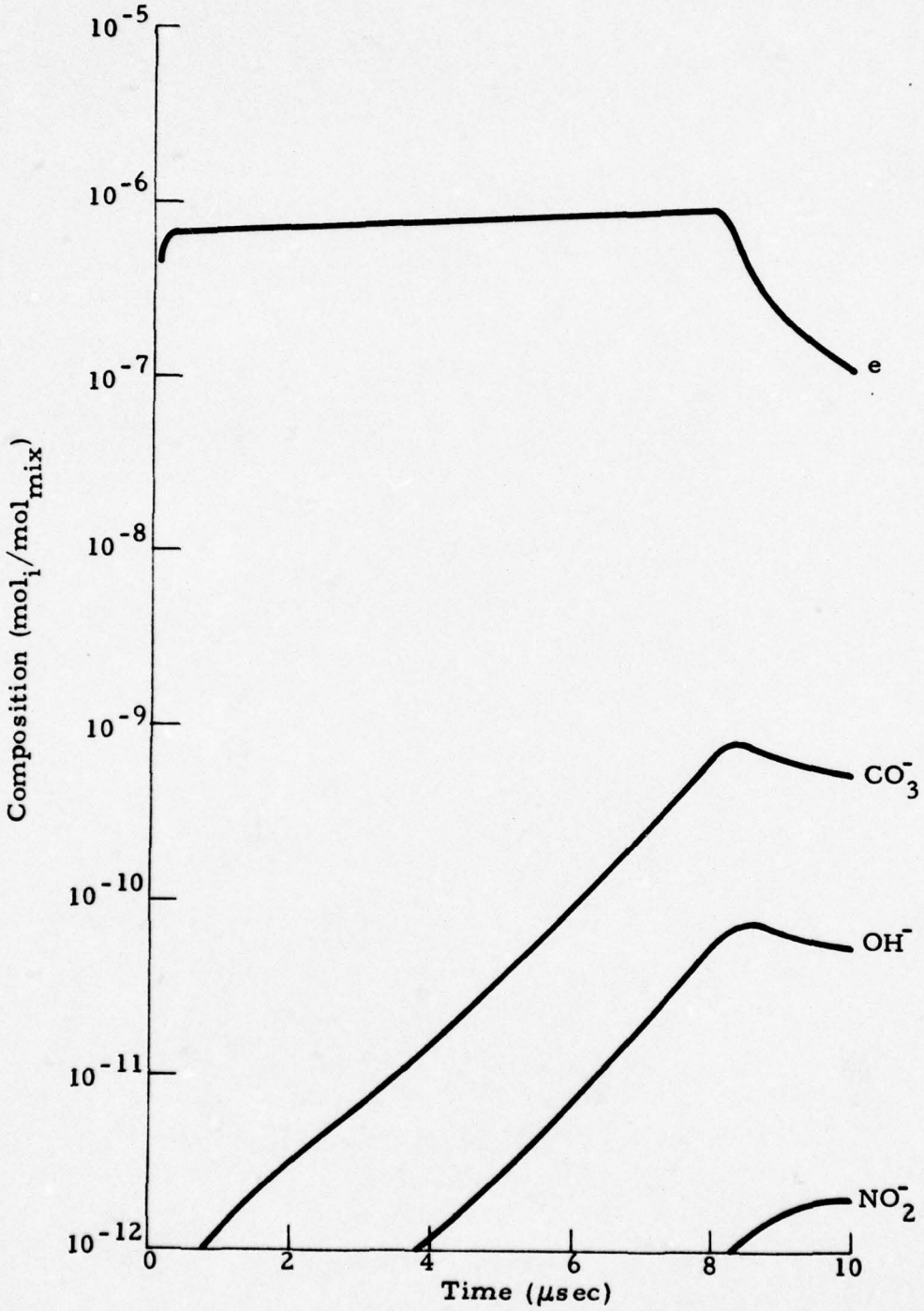

Fig. 10b - $CO_2/N_2/H_2$ = 1/3/0.1; Predicted Single Pulse Temporal Behavior of Major Discharge-Generated Negatively Charged Species

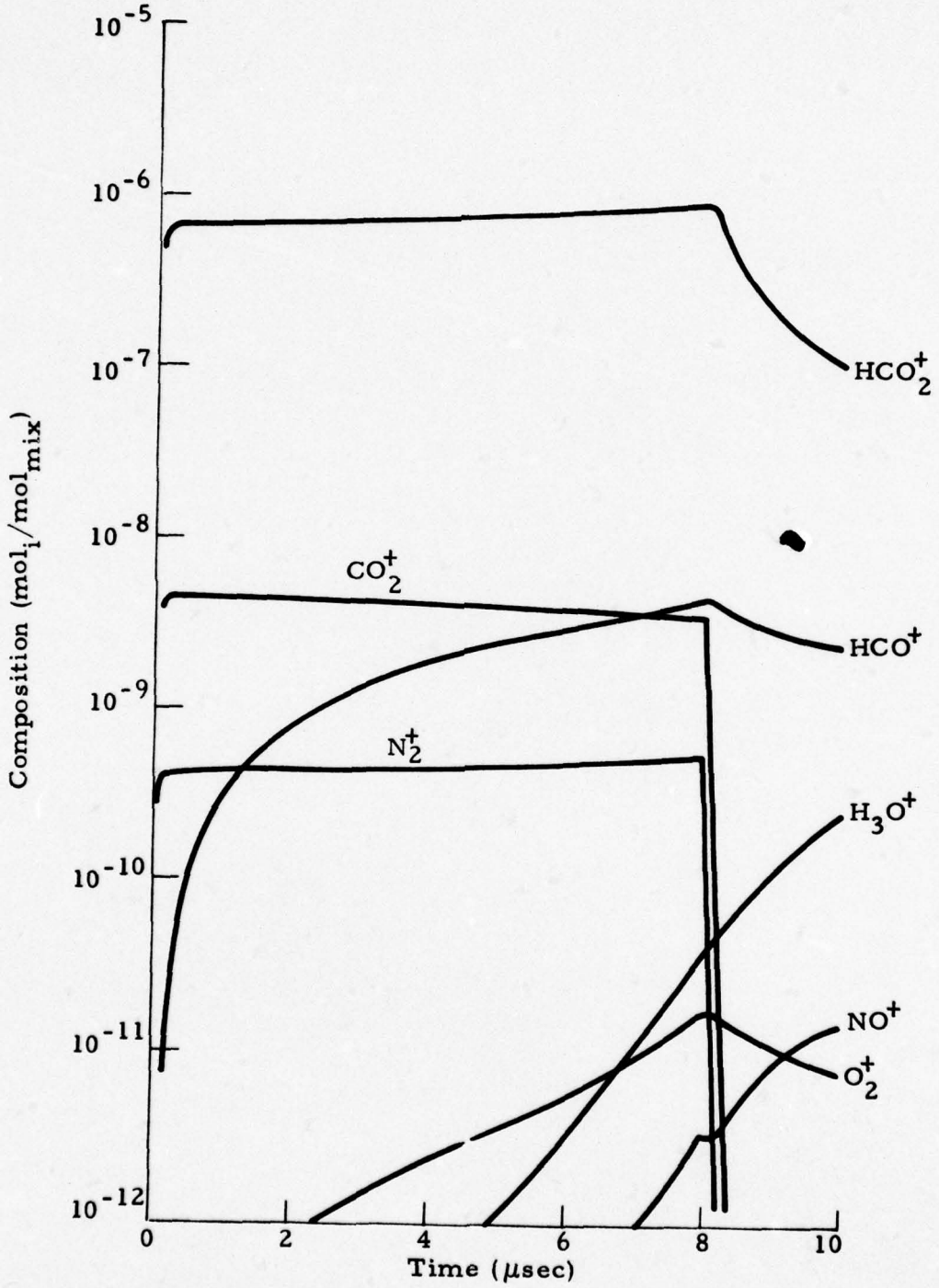

Fig. 10c - $CO_2/N_2/H_2$ = 1/3/0.1; Predicted Single Pulse Temporal Behavior of Major Discharge-Generated Positively Charged Species

must be reassessed constantly as to their validity. It is believed that the results shown in Fig. 10, and in Fig. 10a in particular, may not be entirely correct. The reason is that even small concentrations of certain species can lead to the formation of other species which may become very important. Analysis of the data shown in Fig. 10a led us to believe that the amount of OH formed is sufficient to lead, in conjunction with the NO available, to the formation of HNO_2 (nitrous acid) via the reaction $OH + NO \longrightarrow HNO_2$. Similarly, an even smaller amount of HO_2 (hydroperoxyl) when combined with NO will result in the formation of HNO_3 (nitric acid) via the reaction $HO_2 + NO \longrightarrow HNO_3$. The importance of this realization lies in the fact that both HNO_2 and HNO_3 are strongly electrophilic and may therefore exert an appreciable influence on the free electron distribution. In fact, this may be the very reason for the early decay of the drift field current density in the $CO_2/CO/N_2/H_2$ mixture as shown in Fig. 5 since the analysis of this particular mixture did include the formation of HNO_2 and HNO_3. This is shown in more detail in Figs. 11a through 11c. As can be seen in Fig. 11a, both OH and HO_2 reach the level of one part per million very early in the discharge. With NO already available as a result of hydrocarbon combustion this leads to relatively strong formation of HNO_2 and HNO_3. The other major electrophilic species, O_3 and NO_2 also reach levels of one part per million and almost 20 parts per million, respectively, at the end of the discharge.

Ions formed in the $CO_2/CO/N_2/H_2$ combustion mixture are shown in Figs. 11b and 11c. Among the negative ions, NO_3^- is the only one displaying a positive gradient at the end of the discharge indicating a certain degree of stability. A previous study of a closed cycle continuous wave electric discharge laser (Ref. 2) indicated that NO_3^- was the most stable negative ion. Fig. 11c shows HCO^+ to be the dominant positive ion, and NO^+ to be the second most important one. Again, previous studies indicate that NO^+ is likely to be the most stable positive ion as indicated by its relatively slow decay at the end of the pulse.

With calculations presented here being essentially of exploratory nature it is difficult to reach any firm judgment about the relative merits of the laser

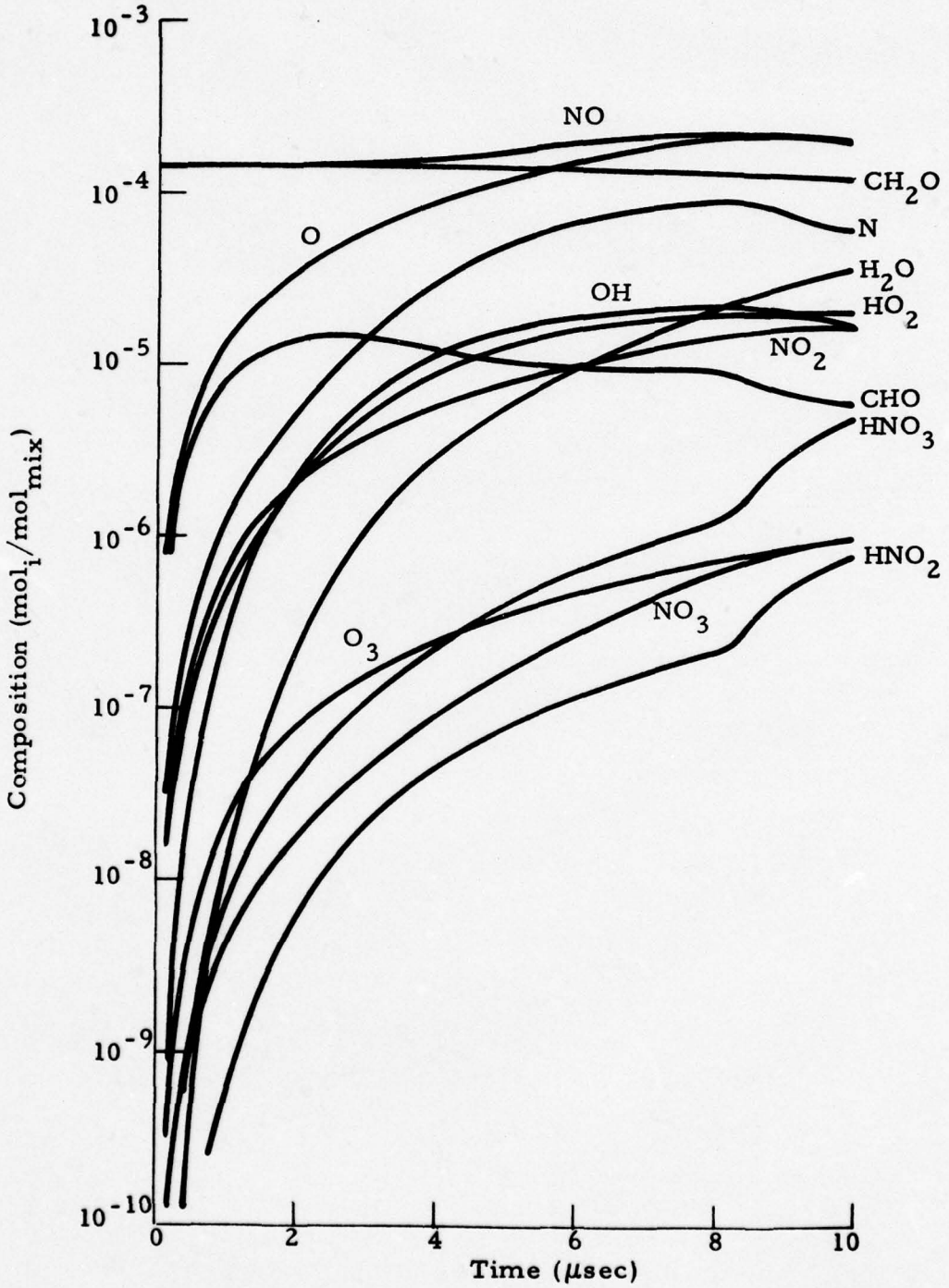

Fig. 11a - $CO_2/CO/N_2/H_2$ = 1/0.25/5.5/0.125; Predicted Single Pulse Temporal Behavior of Major Discharge-Generated Neutral Species

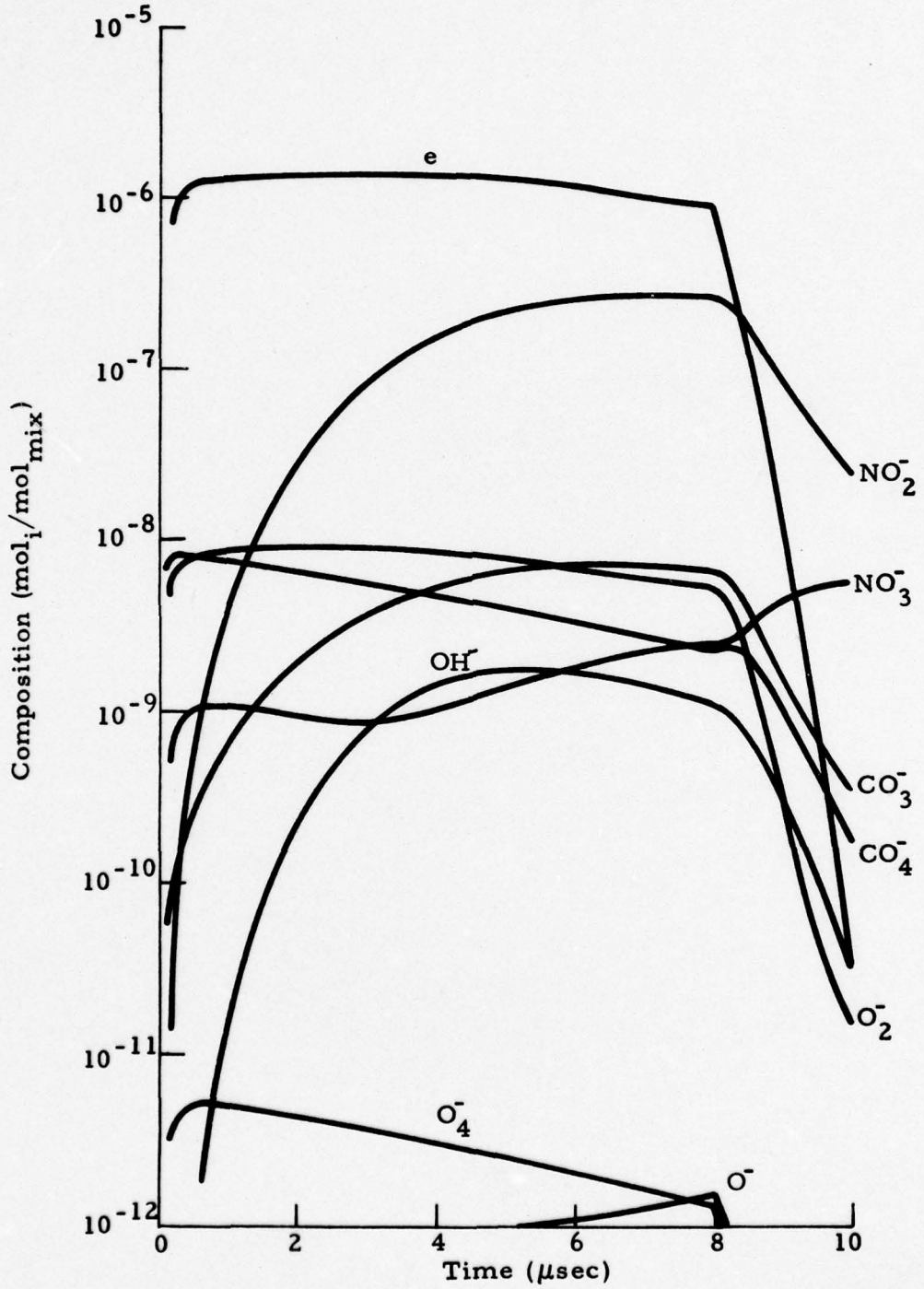

Fig. 11b - $CO_2/CO/N_2/H_2$ = 1/0.25/5.5/0.125; Predicted Single Pulse Temporal Behavior of Major Discharge-Generated Negatively Charged Species

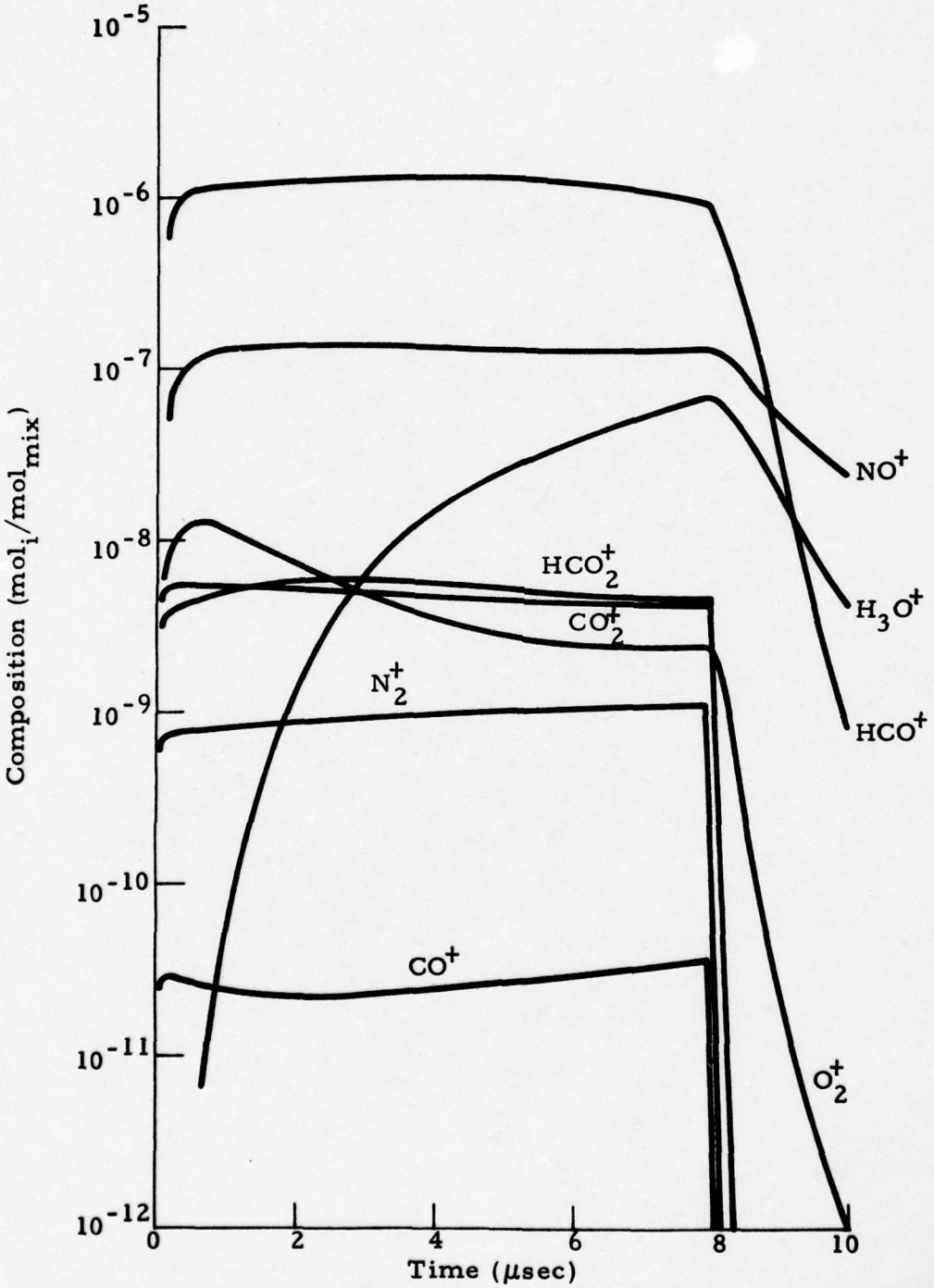

Fig. 11c - $CO_2/CO/N_2/H_2$ = 1/0.25/5.5/0.125; Predicted Single Pulse Temporal Behavior of Major Discharge-Generated Positively Charged Species

gas mixtures discussed. Judging by the peak gain which was predicted it seems that none of the two mixtures containing H_2 can match the performance of the $CO_2/N_2/He$ mixture. However, the peak gain predicted for the $CO_2/CO/N_2/H_2$ mixture is sufficiently high to justify further exploring the concept of laser gas generation via hydrocarbon-air combustion. Much depends on what happens if these mixtures are pulsed repetitively. For example, previous studies (Ref. 2) have indicated that if a $CO_2/CO/N_2/He$ mixture is recirculated through a continuous discharge, steady state performance can easily drop to 50% of single pulse performance even with the use of fresh makeup gas.

Some exploratory calculations of repetitively pulsing the $CO_2/CO/N_2/He$ mixture discussed above are presented next.

3.3 REPETITIVE PULSING AND RECIRCULATION

One of the goals of the present investigation was to shed some light on the response of EDL plasmas when subjected to recirculation and repetitive pulsing. Being of primary interest, the $CO_2/CO/N_2/H_2$ combustion-generated laser gas mixture was analyzed according to the description given in Section 2. The simulated recirculation loop consisted of a discharge pulse of 10 μsec duration, followed by an adiabatic expansion process of 100 μsec duration, followed by an isobaric cooling process of 5 msec duration. This cycle was repeated five times, each cycle starting with the initial conditions of 1 atm and 200 K, and using the gas composition essentially as obtained at the end of the previous cycle. Three variations were analyzed, and their key results are tabulated for easy comparison in Table 5. For Case I, the laser gas was repetitively pulsed without any modification between cycles. As seen in Table 5, a drastic reduction in peak gain and discharge energy density occurred after the first cycle with an attendant shift of the peak gain to the end of the electron beam pulse (at 8 μsec). A moderate rise in both peak gain and discharge energy density commenced with the fourth cycle indicating that after five cycles the plasma was still in a transition phase rather than in a truly repetitive situation.

Table 5

RECIRCULATION AND REPETITIVE PULSING

$CO_2/CO/N_2/H_2$ = 1/0.25/5.5/0.125 Mixture

Case	Cycle	α_{max} (%/cm)	$t_{\alpha_{max}}$ (μsec)	Input (J lit^{-1}-atm^{-1})	Remarks
I	1	2.543	3.7	755.0	No Scrubbing
	2	0.946	8.0	67.6	
	3	0.401	8.0	27.0	
	4	0.416	8.0	28.0	
	5	1.084	8.0	79.5	
II	1	2.543	3.7	755.0	Scrubbing H_2O Only
	2	0.791	8.0	55.4	
	3	0.376	8.0	25.2	
	4	0.44	8.0	29.6	
	5	0.725	8.0	51.0	
III	1	2.543	3.7	755.0	Scrubbing H_2O, HNO_2, HNO_3
	2	2.527	3.7	761.0	
	3	2.522	3.7	761.0	
	4	2.516	3.7	758.0	
	5	2.510	4.0	756.0	

For Case II, the water formed in the discharge (see Fig. 11a) was removed at the end of each cycle, the thought being that any heat exchanger which would cool the gas to 200 K would certainly freeze out any moisture contained in the gas. As the results show, the situation is qualitatively the same as for Case I, and quantitatively even slightly worse as far as reduction of peak gain is concerned. For Case III, not only water but also HNO_2 and HNO_3 formed during the cycle were selectively removed at the end of each cycle, with the result that now the peak gain and its location in time remains practically the same for each cycle and equal to the peak gain of the initial pulse.

The foregoing results clearly establish the fact that the formation of both nitrous and nitric acid play a major role in degrading the plasma in a closed loop EDL using hydrocarbon-air combustion gas as the lasing medium. Figures 12 and 13 serve to further illustrate the results obtained and discussed above. Both figures show on a distorted time scale the temporal concentrations of key contaminants formed during the five cycles. In order to better visualize what happens during each cycle, the first half of each interval on the abscissa represents the discharge of 10 μsec duration, while the second half of each interval represents the remainder of the cycle of approximately 5 msec duration. Figure 12, first of all, shows that once the adiabatic expansion is over all species gradients essentially vanish. This indicates that the plasma is virtually chemically frozen through the remainder of the cycle rendering finite rate calculations in this portion of the cycle largely superfluous. Second considering the temporal behavior of the HNO_3 concentration, which is generally about one order of magnitude higher than the HNO_2 concentration, it can be assumed that it is mainly HNO_3 which causes the deterioration of the gain. Furthermore, low average HNO_3 concentrations over the duration of the discharge pulse appear to correlate well with high peak gain values, and vice versa, which also indicates a close relationship between gain (or electron concentration) and HNO_3 concentration. Otherwise, Fig. 12 shows again that a truly repetitive or steady state has not been reached within five cycles. This is contrasted by the truly repetitive temporal behavior of some key species concentrations shown in Fig. 13 which represents the case where H_2O, HNO_2 and HNO_3 are removed from the gas after each cycle.

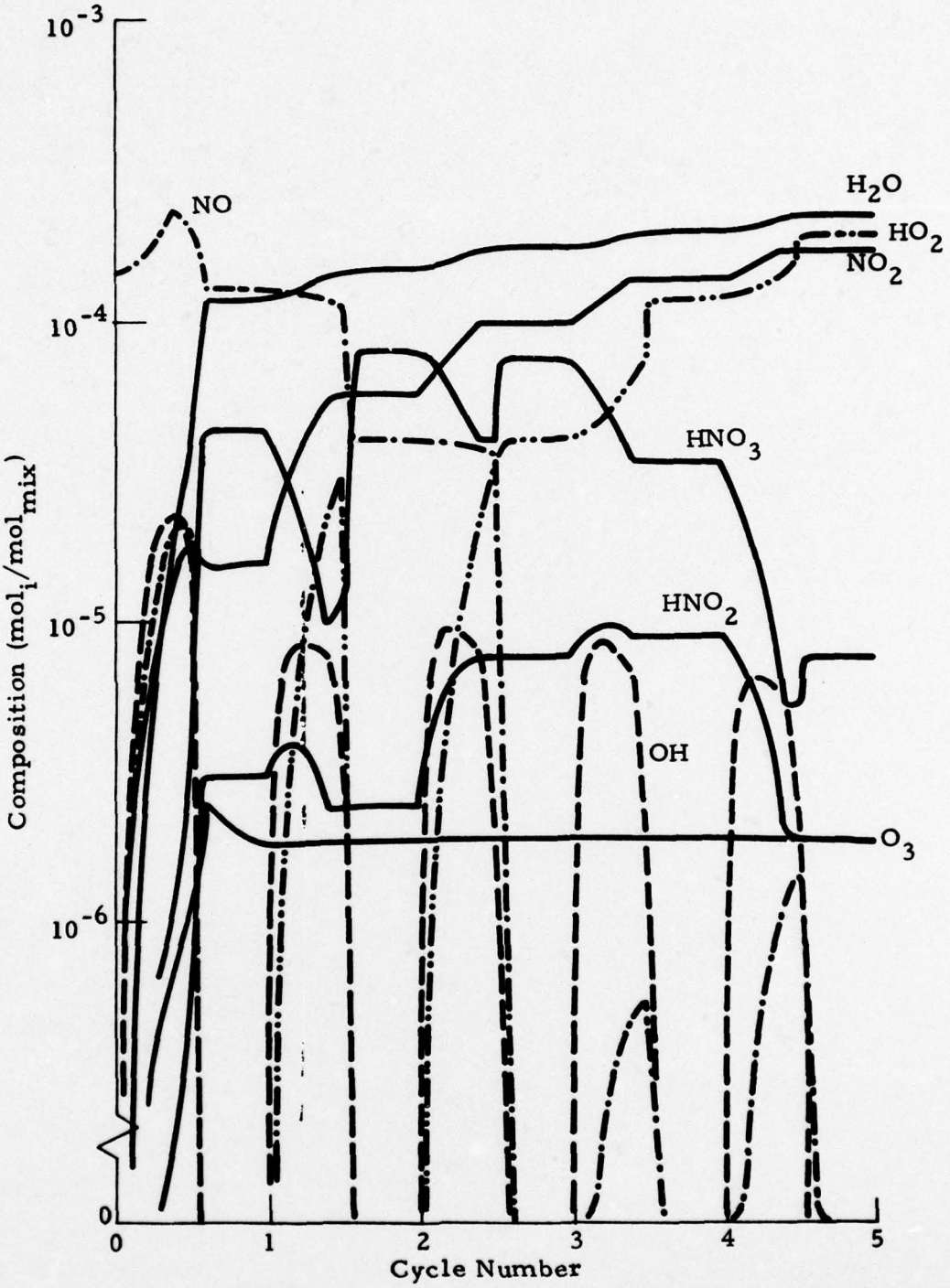

Fig. 12 - $CO_2/CO/N_2/H_2$ = 1/0.25/5.5/0.125; Predicted Temporal Behavior of Selected Discharge-Generated Species Under Closed Cycle and Retetitive Pulsing Conditions

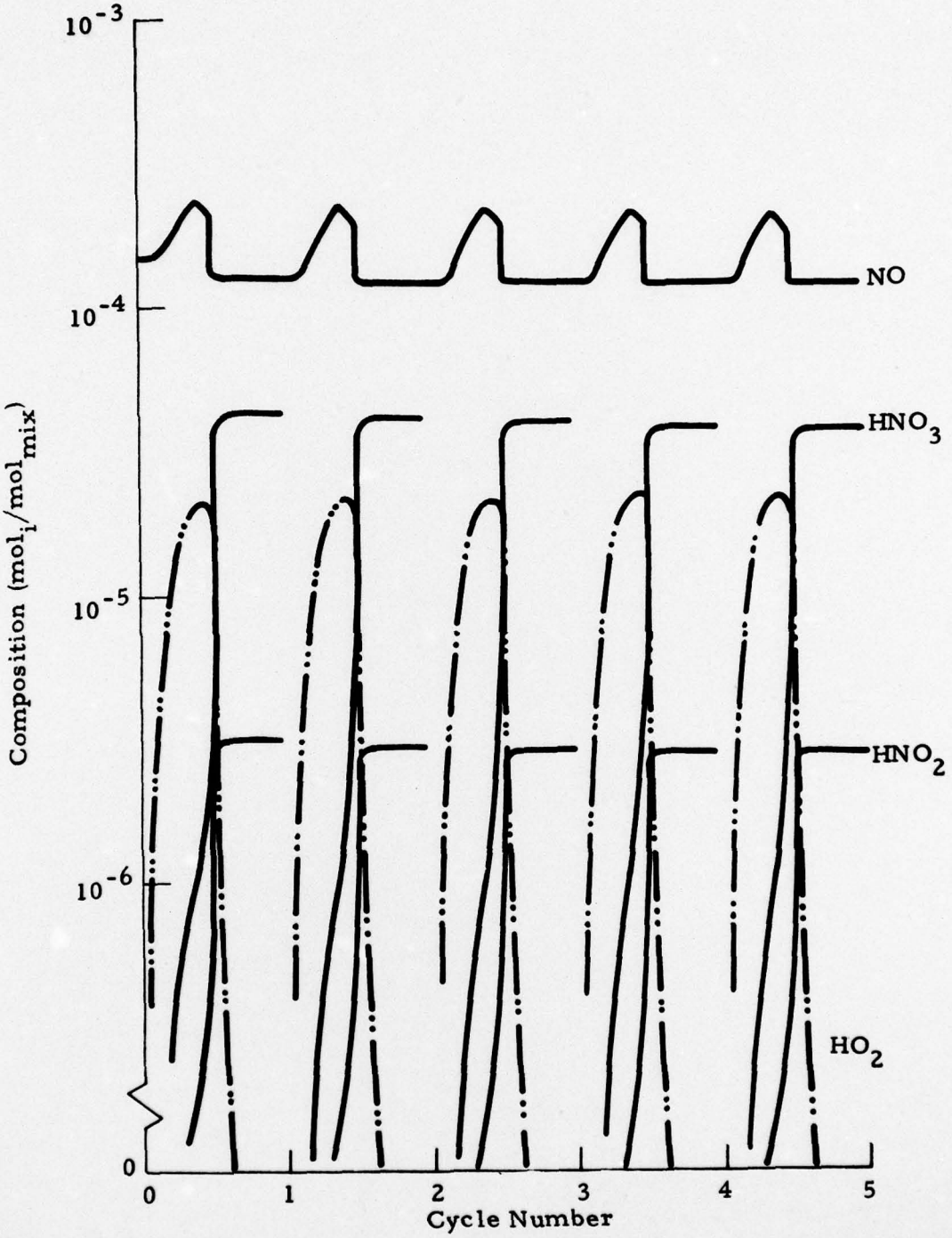

Fig. 13 - $CO_2/CO/N_2/H_2$ = 1/0.25/5.5/0.125; Predicted Temporal Behavior of Selected Discharge-Generated Species Under Closed Cycle and Repetitive Pulsing Conditions with Selective Removal of H_2O, HNO_2 and HNO_3 after Each Cycle

Section 4
CONCLUSIONS AND RECOMMENDATIONS

A theory has been formulated, and a computer code has been developed to investigate the influence of discharge and combustion-produced molecular species on the performance of pulsed electric discharge lasers. As compared to some previous analyses of pulsed CO_2 electric discharge lasers (for example, Refs. 35 through 38), the significance of the analysis presented here lies in the coupling of the detailed plasma chemistry to the other processes of importance in electric discharge laser cavities. Performance models for pulsed electric discharge lasers by Vlases and Moeny (Ref. 35), Kast and Cason (Ref. 36), and Douglas-Hamilton and Lowder (Ref. 38) consider electron and ion concentrations in terms of global coefficients for generation, recombination and attachment but otherwise ignore plasma chemistry effects. According to Wiegand and Nighan (Ref. 39), the model of plasma chemical phenomena developed by Wiegand (Ref. 37 which, however, does not present any details) considers approximately 300 reactions and follows the development of nearly 40 neutral and charged species. However, apparently neither the effects of gas temperature variations nor the process of lasing itself was included.

Theoretical predictions obtained from the present analysis were compared with experimental data for a CO_2 pulsed electric discharge laser using the standard $CO_2/N_2/He$ = 1/2/3 mixture. Encouraging agreement between theory and experiment was obtained for the peak gain and its location in time, as well as for the pulse energy.

Having verified the validity of the theory, the code was applied to a comparative evaluation of two other potential laser gas mixtures. Both mixtures contained H_2 in place of He, and the composition of one mixture was modeled to closely represent a hydrocarbon-air combustion-produced laser gas. Considering the peak unsaturated gain coefficient as a measure of comparison, both mixtures were found to be inferior to the $CO_2/N_2/He$ mixture. Single

pulse peak gain of the $CO_2/N_2/H_2$ mixture was at 52%, and peak gain of the $CO_2/CO/N_2/H_2$ combustion mixture was at 32% of the corresponding value for $CO_2/N_2/He$ mixture under otherwise identical conditions.

The effects on performance of repetitively pulsing a recirculating laser gas mixture, i.e., closed cycle operation, were investigated for the $CO_2/CO/N_2/H_2$ combustion-generated mixture. It was shown that the combination of combustion and discharge-produced contaminants and closed cycle operation may severely degrade laser performance. It was also shown that selective removal of the most important electrophilic reaction products, notably HNO_2 and HNO_3, promises to eliminate the problem of performance degradation. Selective removal of HNO_x can readily be accomplished between passes by passage of the gases over a suitable packed bed of catalyst (e.g., promoted dolomite) since just downstream of the cavity the gas is at the high temperature required to efficiently use this process. This procedure is commonly employed in industrial pollution control using readily available technology and commercial catalysts.

Because of the constraints imposed on the development of the present computer code, namely maximum use of existing kinetic data and of a previously developed CW electric discharge laser code, the program available now is highly specialist-oriented requiring an extremely high degree of familiarity on the side of the user. Applying the code to any large scale or more comprehensive investigation of closed cycle, repetitively pulsed electric discharge lasers would probably be both impractical and uneconomical unless some effort is spent on refining, streamlining and consolidating the program. Such an effort should aim at: (a) the further refinement of the present code to perform detailed analysis of certain cases of particular interest, and (b) developing a "fast" and more efficient program version permitting more global analysis of the essential features of say up to 1000 repetitive pulses by sacrificing a certain amount of detail available from the "standard" version. The above recommended effort should most definitely include further development of the kinetics model. Formidable complexities and uncertainties are involved in modeling the plasma chemistry of CO_2 EDL gas mixtures in depth

sufficient that the formation of electrophilic species concentrations on the order of parts per million can be predicted. In addition to limitations inherent in the information gained from the available literature, value judgments are required with regard to which species and reactions are essential to incorporate in the model. Minimization of the number of species and reaction mechanisms is necessary to hold down the required program core storage and execution time. The latter requirement is especially severe in the analysis of repetitively pulsed lasers for which computations on the order of 1000 pulses might be required.

Confidence in the logic of the assumptions inherent in the program, the need for revisions or extensions and the degree of feasible simplifications derives most productively and directly from further comparison of theoretical and experimental results. A valuable experiment, for example, would be to test the hypothesis stated in Section 3 that HNO_3 might be one of the culprits in degrading closed cycle pulsed EDL performance. Such an experiment, using a mass spectrometer, is currently planned (Ref. 33). Under similar time-averaged conditions the electron concentration is necessarily lower by orders of magnitude in continuous wave operation than it is in pulsed operation. The same likely holds for the HNO_x concentrations which, under CW operating conditions, may be so small as to be undetectable by a mass spectrometer. This situation points to the importance of conducting experiments under pulsed operating conditions.

Continued data analysis and correlation would greatly enhance the significance of performance predictions and as well provide an appreciably greater insight into optimal sustained operation of closed cycle, repetitively pulsed CO_2 high energy lasers.

Section 5
REFERENCES

1. Thoenes, Jürgen, Shelby C. Kurzius, and Marcus L. Pearson, "EDL Performance Model, Part I — Theory and User's Guide," MICOM Technical Report RG-CR-75-2, June 1975.

2. Thoenes, Jürgen and Shelby C. Kurzius, "EDL Performance Model, Part III — Analysis of Closed Cycle Electron-Beam Sustained CO_2 EDL with Air Contaminant," MICOM Technical Report RF-CR-75-2, May 1976.

3. Ellis, H.W., R.Y. Pai, I.R. Gatland, E.W. McDaniel, R. Wernlund and M.J. Cohen, "Ion Identity and Transport Properties in CO_2 Over a Wide Pressure Range," J. Chem. Phys., Vol. 64, 1976, p. 3935.

4. Mitra, A.P., and J.N. Rowe, "Ionospheric Effects of Solar Flares — VI. Changes in D-Region Ion Chemistry During Solar Flares," J. Atmos. Terr. Phys., Vol. 34, 1972, p. 795.

5. Nighan, W.L., and W.J. Wiegand, "Influence of Negative-Ion Processes on Steady-State Properties and Striations in Molecular Gas Discharges," Phys. Rev. A, Vol. 10, 1974, p. 922.

6. Mahan, B.H., and I.C. Walker, "Rate of Attachment of Gaseous Electrons to Nitrogen Dioxide," J. Chem. Phys., Vol. 47, 1967, p. 3780.

7. McFarland, M., D.L. Albritton, F.C. Fehsenfeld, E.E. Ferguson, and A.L. Schmeltekopf, "Flow Drift Technique for Ion Mobility and Ion Molecule Reaction Rate Constant Measurements, III. Negative Ion Reactions of O^- with CO, NO, H_2 and D," J. Chem. Phys., Vol. 59, 1973, p. 6629.

8. Ferguson, E.E., "Rate Constants of Thermal Energy Binary Ion-Molecule Reactions of Aeronomic Interest," Atomic Data and Nuclear Data Tables, Vol. 12, 1973, p. 159.

9. Spjeldvik, W.N., and Thorne, R.M., "A Simplified D-Region Model and Its Application to Magnetic Storm After-Effects," J. Atmos. and Terr. Phys., Vol. 37, 1975, p. 1313.

10. Fehsenfeld, F.C., and E.E. Ferguson, "Laboratory Studies of Negative Ion Reactions with Atmospheric Trace Constituents," J. Chem. Phys., Vol. 61, 1974, p. 3181.

11. Bates, D.R., and A. Dalgarno, "Electronic Recombination," in Atomic and Molecular Processes (Ed. D.R. Bates), (Academic Press, New York), 1962, pp. 245-279.

12. Biondi, M.A., "The Effects of Ion Complexity on Electron-Ion Recombination," Comments on Atomic and Molecular Physics, Part D, 1974, p. 85.

13. Kasner, W.H., and M.A. Biondi, "Temperature Dependence of the Electron – O_2^+ Ion Recombination Coefficient," Phys.Rev., Vol. 174, 1968, p. 139.

14. Hansen, C.F., "Temperature Dependence of the NO^+ + e Dissociative Recombination Rate Coefficient," Phys. Fluids, Vol. 11, 1968, p. 904.

15. Moseley, J.T., R.E. Olson, and J.R. Peterson, Case Studies in Atomic Physics, Vol. 5, Eds. E.W. McDaniel, and M.R.C. McDowell, (Amsterdam: North Holland), 1975, pp. 1-45.

16. Flannery, M.R., "Ionic Recombination" (in press).

17. Nighan, W.L., "Electron Energy Distributions and Collision Rates in Electrically Excited N_2, CO and CO_2," Phys. Rev. A, Vol. 2, 1970, p. 1989.

18. Douglas-Hamilton, D.H., R.M. Feinberg, R.S. Lowder, J.P. Roos and O.L. Zappa, "High Specific Energy Pulsed Electric Discharge Laser Research," Avco-Everett Research Laboratory, Final Technical Report on Contract DAAH01-75-C-0503, December 1975.

19. Fehsenfeld, F.C., C.J. Howard and A.L. Schmeltekopf, "Gas Phase Ion Chemistry of HNO_3," J. Chem. Phys., Vol. 63, 1975, p. 2835.

20. Ferguson, E.E., "Laboratory Measurements of Ionospheric Ion-Molecule Reaction Rates," Rev. Geophys. Space Phys., Vol. 12, 1974, p. 703.

21. Fehsenfeld, F.C., "Reaction of CO_3^-, NO_3^-, and CO_4^- with Atomic Hydrogen," J. Chem. Phys., Vol. 63, 1975, p. 1686.

22. Hurle, I.R., T.M. Sugden, and G.B. Nutt, "Chemi-Ionization of Nitric Oxide in Flames Containing Hydrocarbon Additives," Twelfth Symposium (International) on Combustion, The Combustion Institute, Pittsburgh, Pa., 1969, p. 387.

23. Pritchard, H., and G. Harrison, "Ion-Molecule Reactions of Oxygenated Species. Proton-Transfer Reactions Involving CHO^+," J. Chem. Phys., Vol. 48, 1968, p. 5623.

24. Calcote, H.F., S.C. Kurzius and W.J. Miller, "Negative and Secondary Ion Formation in Low-Pressure Flames," Tenth Symposium (International) on Combustion, The Combustion Institute, Pittsburgh, Pa., 1965, p. 605.

25. Stricker, J., "Deactivation of $CO_2(010)$ and $CO_2(001)$ by Hydrogen and Deuterium," J. Chem. Phys., Vol. 64, 1976, p. 1261.

26. Kurzius, S.C., "LAMP Reaction Models for Analysis of Chemical Lasers," MICOM Technical Report RK-CR-75-31, Vol. III, June 1975.

27. Shimazaki, T., and T. Ogawa, "A Theoretical Model of Minor Constituent Distributions in the Stratosphere Including Diurnal Variations," J. Geophys. Res., Vol. 79, 1974, p. 3411.

28. Shimazaki, T., and R.C. Whitten, "A Comparison of One-Dimensional Theoretical Models of Stratospheric Minor Constituents," Rev. Geophys. and Space Phys., Vol. 14, 1976, p. 1.

29. Baulch, D.L., D.D. Drysdale and D.G. Horne, Evaluated Kinetic Data for High Temperature Reactions — Vol.2, Homogeneous Gas Phase Reactions of the H_2-N_2-O_2 System (Butterworth, London, 1973).

30. Wuebbles, D.J., and J.S. Chang, "Sensitivity of Time-Varying Parameters in Stratospheric Modeling," J. Geophys. Res., Vol.80, 1975, p.2637.

31. Dezenberg, George J., Charles Cason and Robert J. Huff, "Gain Coefficient and Output Energy Characteristics of a High Pressure Pulsed CO_2 Laser," Technical Digest, 1973 International Electron Devices Meeting, Washington, D.C., 3-5 December 1973.

32. Cason, Charles, George J. Dezenberg and Robert J. Huff, "Operation of a Cold-Cathode Electron-Beam-Controlled CO_2 Laser Oscillator at 1-3 Atm," Appl. Phys. Lett., Vol.23, No.2, 15 July 1973, p.110.

33. Cason, Charles M., Personal Communication, 1976.

34. Cason, Charles et al., "A Small Scale Closed Cycle Circulator Experimental Plan for Repetitively Pulsed 200 K High Pressure Electric Discharge Lasers," MICOM Technical Report RH-76-12, 2 August 1976.

35. Vlases, George C., and William M. Moeny, "Numerical Modeling of Pulsed Electric CO_2 Lasers," J. Appl. Phys., Vol.43, No.4, April 1972, p.1840.

36. Kast, Steven J., and Charles Cason, "Performance Comparison of Pulsed Discharge and E-beam Controlled CO_2 Lasers," J. Appl. Phys., Vol.44, No.4, April 1973, p.1631.

37. Wiegand, W.J., Bull. Am. Phys. Soc., Vol.17, 1972, p.398.

38. Douglas-Hamilton, D.H., and R.S. Lowder, "AERL Kinetics Handbook," Avco Everett Research Laboratory, Everett, Mass., July 1974.

39. Wiegand, W.J., and William L. Nighan, "Plasma Chemistry of CO_2-N_2-He Discharges," Appl. Phys. Lett., Vol.22, No.11, 1 June 1973, p.583.

REPORTS DISTRIBUTION LIST

1.	Defense Advanced Research Project Agency 1400 Wilson Blvd. Arlington, VA 22209 Attn: Director, Laser Division	1
2.	ODDR&E The Pentagon Washington, DC 20301 Attn: Assistant Director (Space and Advanced Sys.)	1
3.	National Aeronautics and Space Administration Lewis Research Center 21000 Brookpark Road Cleveland, OH 44135 Attn: Dr. John W. Dunning, Jr.	1
4.	Defense Documentation Center Cameron Station Alexandria, VA 22314	2
5.	Department of the Army DCSRDA Washington, D.C. 20310 Attn: DAMA-WMS-A (LTC Holmes)	1
6.	Commander US Army Missile Command Redstone Arsenal, AL 35809 Attn: AMSMI-RHS, Mr. Charles Cason	5
7.	Commander US Army Missile Command Redstone Arsenal, AL 35809 Attn: AMCPM-HEL	3
8.	Commander US Army Mobility Equipment R&D Center Ft. Belvoir, VA 22060 Attn: AMXFB-EA (L. Amstutz)	1
9.	Commander US Army Materiel Command 5001 Eisenhower Avenue Alexandria, VA 22304 Attn: AMCRD (Dr. David Stefanye)	1

10. Commander — 1
US Army Electronics Command
Ft. Monmouth, NJ 07703

Attn: AMSEL-CT-L (Dr. R.G. Buser)

11. Naval Sea Systems Command — 1
PMS 405
Washington, DC 20362

Attn: CPT James G. Wilson
Project Mgr, High Energy Laser Project

12. Air Force Weapons Laboratory — 1
Kirtland AFB, NM 87117

Attn: COL Donald L. Lambertson (AR)

13. AF Aero Propulsion Laboratory — 1
Wright Patterson AFB, OH 45433

Attn: MAJ George Uhlig (AFAPL/NA)

14. Aerospace Corp. — 1
P.O. Box 92957
Los Angeles, CA 90009

Attn: Dr. Walter Warren

15. Airesearch Manuf. Co. — 1
2525 West 190th Street
Torrance, CA 90503

Attn: Mr. A. Colin Stancliffe

16. AVCO-Everett Res. Lab. — 2
2385 Revere Beach Parkway
Everett, MA 02149

Attn: Dr. Jack Daugherty

11. Battelle Columbus Laboratories — 1
505 King Ave.
Columbus, OH 43201

Attn: Mr. Fred Tietzel (STOLAC)

18. Hughes Research Laboratories — 1
3011 Malibu Canyon Road
Malibu, CA 90265

Attn: Dr. Arthur N. Chester

19. Hughes Aircraft Co. 1
Centinela and Teale Streets
Culver City, CA 90230

Attn: Dr. Eugene Peressini (Bldg. 6, MS/E-125)

20. Lawrence Livermore Lab 1
P.O. Box 808
Livermore, CA 94550

Attn: Dr. John Emmett

21. Los Alamos Scientific Laboratories 1
P.O. Box 1663
Los Alamos, NM 87544

Attn: Dr. Keith Boyer (MS 530)

22. Mathematical Sciences Northwest, Inc. 1
4545 15th Ave., NE
Seattle, WA 98105

Attn: Mr. Peter H. Rose

23. Massachusetts Institute of Technology 1
Lincoln Laboratory
P.O. Box 73
Lexington, MA 02173

Attn: Dr. Rediker

24. Northrop Corp. 1
3401 West Broadway
Hawthorne, CA 90250

Attn: Dr. Gerard Hasserjian

25. Rockwell International Corp. 1
Rocketdyne Division
6637 Canoga Ave.
Canoga Park, CA 91304

Attn: Marc T. Constantine

26. Science Applications, Inc. 1
6666 Powers Ferry Road, Suite 202
Atlanta, GA 30339

Attn: Mr. Harvey Ford

27. Systems, Science and Software 1
P.O. Box 1620
LaJolla, CA 92037

Attn: Mr. Alan F. Klein

28. United Aircraft Res. Lab. 1
400 Main St.
East Hardford, CT 06108

Attn: Mr. G.H. McLafferty

29. Westinghouse Electric Corp. 1
Defense and Space Center
Friendship International Airport - Box 746
Baltimore, MD 21203

Attn: Mr. W.F. List

37